Society for Mathematical Biology

A Mathematical Model of the Effects of Aging on Naive T Cell Populations and Diversity

Stephanie Lewkiewicz[1] · Yao-li Chuang[2,3] · Tom Chou[1,3]

Abstract

The human adaptive immune response is known to weaken in advanced age, resulting in increased severity of pathogen-born illness, poor vaccine efficacy, and a higher prevalence of cancer in the elderly. Age-related erosion of the T cell compartment has been implicated as a likely cause, but the underlying mechanisms driving this immunosenescence have not been quantitatively modeled and systematically analyzed. T cell receptor diversity, or the extent of pathogen-derived antigen responsiveness of the T cell pool, is known to diminish with age, but inherent experimental difficulties preclude accurate analysis on the full organismal level. In this paper, we formulate a mechanistic mathematical model of T cell population dynamics on the immunoclonal subpopulation level, which provides quantitative estimates of diversity. We define different estimates for diversity that depend on the individual number of cells in a specific immunoclone. We show that diversity decreases with age primarily due to diminished thymic output of new T cells and the resulting overall loss of small immunoclones.

✉ Tom Chou
tomchou@ucla.edu

Stephanie Lewkiewicz
slewkiewicz@math.ucla.edu

Yao-li Chuang
ylch07@gmail.com

[1] Department of Mathematics, UCLA, Los Angeles, CA 90095-1555, USA

[2] Department of Mathematics, CalState-Northridge, Northridge, CA 91330-8313, USA

[3] Department of Biomathematics, UCLA, Los Angeles, CA 90095-1766, USA

Springer

1 Introduction

Immunosenescence underlies poor health outcomes in the aging population, including diminished vaccine efficacy (Poland et al. 2010; McElhaney and Dutz 2008; Fleming and Elliot 2008), increased susceptibility to disease (including irregular presentation, intensified symptoms, longer recovery times, increased mortality) (Thomas-Crussels et al. 2012), and a heightened risk of cancer (Ginaldi et al. 2001). This degradative aging process of the human immune system originates from extensive fundamental changes to the size and functionality of immune cell pools, and the structure of lymphatic tissues in which they develop and operate (Salam et al. 2013).

Among the many changes associated with immunosenescence (Globerson and Effros 2000), the T cell compartment is arguably the most damaged (Wick et al. 2000; Gruver et al. 2007). The T cell pool is comprised of subpopulations of antigen-inexperienced naive cells and antigen-experienced memory cells, the latter of which retain immunological record of previous infections. The human immune compartment maintains $\sim 10^{12}$ T cells in total, of which $\sim 10^{11}$ are naive (Jenkins et al. 2009; Trepel 1974). During aging, the population of naive T cells declines in overall size, while the population of memory T cells undergoes extensive proliferation, thereby reversing the balance of naive and memory T cells that had persisted at younger ages (Globerson and Effros 2000; Fagnoni et al. 2000). The expansion of memory T cells further enhances immunological memory of previously encountered antigens, reinforcing existent immune protection. The remaining naive pool experiences loss of T cell receptor (TCR) "structural diversity" (Goronzy et al. 2007, 2015b)—the number of distinct TCR complexes present across the entire naive pool. The diversity of T cell clones, or "immunoclones," characterized by the number of distinct TCR complexes among the cell population, provides the extent of antigen specificity. Unique TCR complexes are generated during T cell development in the thymus, via recombination of genes encoding the V and J domains of the TCRα chain and the V, J, and D domains of the TCRβ chain, along with additional insertion and deletion of nucleotide fragments (Murphy 2012). Combinatorially, a possible $\Omega_0 \sim 10^{15}$–10^{20} unique TCR complexes may be assembled via this rearrangement process (Laydon et al. 2015), but only $\Omega \sim (0.05) \times \Omega_0$ of those rearrangements are functionally viable (Yates 2014), as determined by positive and negative selection tests in the thymus, which screen for appropriate reactivity to self-peptide/MHC molecules. Each TCR is activated by at least one peptide fragment presented via MHC molecules on the surface of an antigen-presenting cell; thus, loss of naive TCR structural diversity limits the number of new antigens to which the full naive T cell pool can respond. Naive cells are also suspected to suffer major functional deficiencies in aging, such as diminished binding affinity and proliferative capacity after antigenic stimulation (Moro-García et al. 2013), which have been studied mostly using murine models to date (Appay and Sauce 2014). Their effects on human immune systems are not yet well understood but nonetheless beyond the scope of this paper.

The total abundance of naive T cells, which inhabit both blood and lymphatic tissue, can be reliably estimated from measurements in small samples (Westermann and Pabst 1990; Bains et al. 2009a). Recently, Westera et al. (2015) estimated an $\sim 52\%$ decrease in the naive T cell population in aging. In contrast, accurate estimation of full-

organism TCR structural diversity is currently impeded by experimental imprecision and the inability to extrapolate small sample data to the full organism (Laydon et al. 2015). Experimentation typically entails DNA sequencing of the TCRα or—more commonly—β chain, in particular the complementarity-determining region 3 (CDR3), which is the site of TCR binding to antigenic peptide and most significant basis for diversity (Murphy 2012).

Increasingly sophisticated sequencing and analysis methods have improved estimates (Shugay et al. 2015; Oakes et al. 2017) for the lower bound on TCR diversity, but direct estimation of TCR diversity remains a challenge due to various experimental complications, such as the inability to detect rare clonotypes, sequencing errors, and inaccurate measurement of clonotype frequencies resulting from inconsistencies in polymerase chain reaction (PCR) amplification (Laydon et al. 2015). Predicting full-organism TCR diversity from a small sample is typically formulated as an "unseen species problem," and one of many canonical solutions to such a problem is employed in conjunction with experimental data (Chao 1984; Chao and Lee 1992; Colwell and Coddington 1994), but the true relationship between sample and full diversity is fundamentally elusive.

Despite variations across experimental measurements of TCR diversity, its age-related loss has been consistently observed. An early study conducted by Naylor et al. (2005) predicted a TCRβ chain diversity of $\sim 2 \times 10^7$ that persisted in donors through age 60, before dropping by two orders of magnitude to $\sim 2 \times 10^5$ at age 70. More recently, Britanova et al. (2014) collected samples from donors of all ages and observed an approximately linear decrease in TCRβ CDR3 diversity from $\sim 7 \times 10^6$ in youth (6–25 years) to $\sim 2.4 \times 10^6$ in advanced age (61–66 years). Qi et al. (2014) obtained a particularly high lower bound estimate of $\sim 10^8$ unique TCRβ sequences in youth (20–35 years), which declined two- to fivefold in advanced age (70–85 years).

Note that only the TCRβ chain is sequenced in these experiments. Sequencing of both the α and β chains would potentially produce a more accurate measure of TCR diversity, but the same experimental limitations preclude complete analysis. The measurement of diversity is further complicated by the potentially large disparity between structural diversity and "functional diversity"—that is, the number of antigens to which the T cell pool is capable of responding. Due to the potential for crossreactivity, in which one TCR might respond to many structurally similar peptide fragments, it is possible that actual TCR diversity is much higher than structural diversity indicates. It has been speculated that one TCR might respond to as many as 10^6 different peptide epitopes (Mason 1998).

To obtain lifetime estimates of TCR structural diversity and develop an informed context for discussion of functional diversity, we introduce a mechanistic mathematical model of the generation and replenishment of the naive T lymphocyte pool from birth through the end of life. Although experimental assessments of full-system information remain challenging, measurements for the dynamics of each component related to the naive T cell population can be found throughout the literature. Our mathematical approach combines the knowledge of these individual components to study their interplay, leading to an understanding of the full-system dynamics. By extending previous model studies of total cell counts (Mehr et al. 1996, 1997; Ribeiro and Perelson 2007; Bains et al. 2009a, b; Hapuarachchi et al. 2013; Murray et al. 2003; Reynolds et al.

2013), our multi-component formulation is able to efficiently track the total number of distinct naive T cell clones, allowing for a full-system assessment of TCR structural diversity.

2 Mathematical Models and Results

We develop our mathematical model by first constructing the equation governing the total population size of the naive T cell pool in Sect. 2.1, through which we quantitatively constrain the primary parameters of our model using experimental measurements found in the previous literature. The model that describes the evolution of immunoclones is derived in Sect. 2.2, allowing us to define and estimate the diversity of the naive T cell population in Sect. 2.3. In Sect. 2.4, we inspect the impact of sampling on the estimate of immunoclone diversity, as in practice it is only possible to extract a small fraction of the entire naive T cell population from a body.

2.1 Total Naive T Cell Population Model

There are three fundamental immunological mechanisms that sustain the naive T cell pool: (1) export of mature naive T cells from the thymus, (2) peripheral proliferation, and (3) cell removal from the naive pool due to death or phenotypic changes. These basic mechanisms constitute a birth–death–immigration process described by the ordinary differential equation:

$$\frac{\mathrm{d}N(t)}{\mathrm{d}t} = \gamma(t) + pN(t) - \mu(N)N(t), \tag{1}$$

where $N(t)$ denotes the total naive T cell count, $\gamma > 0$ denotes the rate of thymic output, $p > 0$ denotes the rate of proliferation, and $\mu(N) > 0$ denotes the rate of population-dependent regulated cellular death or loss of naive phenotype.

While more complex feedback mechanisms have been proposed (Mehr et al. 1997), other experiments have shown that thymic export is independent of naive T cell counts (Ribeiro and Perelson 2007; Berzins et al. 1998; Metcalf 1963) and it is well established that the export rate consistently decays throughout the human lifespan (Murray et al. 2003). The lifelong decline of thymic export is caused by thymic involution and leads to the degradation of structural integrity and functional capacity of the thymus with age (Steinmann et al. 1985). The age dependence of the thymic export rate of newly trained naive T cells is often approximated by an exponentially decaying function, $\gamma(t) = \gamma_0 e^{-at}$, where $\gamma_0 > 0$ is the maximum rate of thymic output that arises in early years and $a > 0$ is the rate of decrease in thymic output.

The immune systems of vertebrates maintain a healthy amount of naive T cells through complex homeostatic mechanisms, which include controlled production and distribution of common gamma chain cytokines, particularly IL-7, to the naive pool (Fry and Mackall 2005). IL-7 is secreted by stromal and endothelial cells in the thymus, bone marrow, and lymphatic tissue, providing T cells with necessary survival signals. In lymphoreplete conditions, competition for this limited resource

regulates population size (Bradley et al. 2005; Tan et al. 2001; Vivien et al. 2001), but in lymphopenic conditions, high levels of IL-7 resulting from low T cell counts can even stimulate cellular proliferation. While IL-7 concentration may be explicitly formulated in a mathematical model of the peripheral T cell population, as in the work of Reynolds et al. (2013), most models incorporate IL-7 regulation implicitly in the form of carrying capacity, assuming quick equilibration in a state of competition for IL-7 in the presence of a given number of T cells. Such simplification commonly leads to the dependence on total cell counts of both cell proliferation and cell death rates, considering the cytokine's dual role under lymphoreplete and lymphopenic conditions described above. Our model assumes a cell count dependence in the cell death rate only, focusing on scenarios of *healthy* aging, i.e., lymphoreplete conditions. We thus assume a regulated N-dependent cell death rate of the form

$$\mu(N) = \mu_0 + \frac{\mu_1 N^\theta}{N^\theta + K^\theta}, \tag{2}$$

where the first term, $\mu_0 > 0$, is the basal rate of cellular death. The second one describes the IL-7-mediated regulation of cell death, with $\mu_1 > 0$ representing the maximal increase to the death rate as $N \to \infty$. The quantity K is analogous to a "carrying capacity" and dictates the population at which signaling-induced death starts to limit the population. We have shown that model predictions are not qualitatively sensitive to the Hill coefficient, so without loss of generality we fix the Hill coefficient $\theta = 2$.

The constant rate of cellular proliferation p under healthy conditions is supported by recent studies of Westera et al. (2015), showing nearly identical naive proliferation rates at young and old ages during age-related nonlymphopenic loss of naive cells. IL-7-induced proliferation can arise in *unhealthy* lymphopenic conditions typically found in severe disease of the immune system (Brass et al. 2014), cytotoxic drug use (Gergely 1999), radiation treatment (Grossman et al. 2015), or other abnormal situations. These scenarios are, however, beyond the scope of our analysis.

Our model has six adjustable parameters, γ_0, a, p, μ_0, μ_1, and K. The first four are biologically inherent to the mechanism of T cell homeostasis and have been measured experimentally in humans and rodents. The last two have to be constrained via parameter sweeps to match relevant experimental observations. To non-dimensionalize Eqs. 1, 2, we use a^{-1} to rescale t and K to rescale N to find

$$\frac{\mathrm{d}N'}{\mathrm{d}t'} = \frac{\gamma_0}{aK}\mathrm{e}^{-t'} + \frac{(p - \mu_0)}{a}N'\left(1 - \frac{\mu_1}{(p - \mu_0)}\frac{N'^2}{N'^2 + 1}\right) \tag{3}$$

which depends on the three independent parameters, $\gamma_0/(aK)$, $(p - \mu_0)/a$, and $\mu_1/(p - \mu_0)$, that control the qualitative behavior of our model. Specifically, the parameter $\mu_1/(p - \mu_0)$ specifies how quickly the N-dependent death rate approaches its maximal value. Note that p and μ_0 always appear together in the form of $(p - \mu_0)$ in the model and thus are effectively just one parameter, reducing the number of free parameters by one.

Figure 1a illustrates four qualitatively distinct evolution trajectories of $N(t)$ that may arise from simulations of the model in the presence of a decaying thymic export rate $\gamma(t)$ (gray dashed–dotted curve). The black dashed curve arises when $\mu_1/(p - \mu_0) < 1$. In this case, cell proliferation always exceeds cell death, leading to unbounded expansion of the naive T cell population. This scenario is unrealistic, except perhaps during a period of lymphopenia. For $\mu_1/(p - \mu_0) \geq 1$, cell death is able to balance cell proliferation at a homeostatic carrying capacity $N = N_{ss}(\gamma = 0)$, defined by $\mu(N_{ss}(\gamma = 0)) = p$, as $\gamma \to 0$. As illustrated by the green dotted curve, $N(t)$ rises and asymptotically converges toward $N_{ss}(\gamma = 0)$ provided that $\gamma_0/(aK) \ll 1$. We refer to this scenario as being in the "proliferation-driven" regime, given that the cell population is driven to $N_{ss}(\gamma = 0)$ primarily by homeostatic proliferation. The model's behavior makes a transition from proliferation driven to "thymus driven" if we increase $\gamma_0/(aK)$. As shown by the blue solid curve, $N(t)$, driven by increased thymic export, overshoots and approaches $N_{ss}(\gamma = 0)$ from above as $\gamma(t) \to 0$ asymptotically. In "Appendix A," we define "direct thymic output" and "proliferation-generated" subpopulations of naive T cells. A thymus-driven description indicates that the lifetime evolution of $N(t)$ is entrained by thymic involution. We show that even in this case, the majority of the naive T cell population is maintained by homeostatic proliferation, while cells directly exported from the thymus only comprise 10–25% of the population, consistent with previous experimental findings in human adults (den Braber et al. 2012.)

Finally, the red dashed–dotted curve arises when $(p - \mu_0)/a \leq 0$. In this case, cell death always exceeds cell proliferation as $\gamma(t) \to 0$. In this case, the naive T cell population is almost entirely sustained by direct thymic export, and $N(t) \to N_{ss}(\gamma = 0) = 0$. This scenario is consistent with previous experimental findings in mice, where the average lifespan of naive T cells is shorter than cell doubling time, rendering peripheral proliferation of naive T cells highly unlikely in mice (den Braber et al. 2012). As stated earlier, in this paper we focus on scenarios of healthy aging (lymphoreplete conditions) in humans, which immediately rules out the scenarios of unbounded growth (black dashed curve) and complete collapse of the T cell population (the red dotted–dashed curve), effectively constraining our parameters to the physiologically reasonable values $\mu_1/(p - \mu_0) \geq 1$ and $(p - \mu_0)/a > 0$.

We can further quantitatively calibrate the parameter values using experimental measurements for human adults in the literature. The constant peripheral proliferation rate p has been measured by Westera et al. (2015) as 0.05% day^{-1}, or equivalently $p = 0.18$ year^{-1} in a healthy human. The basal death rate μ_0 can be estimated from the lifespan of T-cells. Based on data from Vrisekoop et al. (2008), De Boer and Perelson (2013) obtain an average naive human CD4$^+$ T-cell lifespan of ~ 5 years and an average naive human CD8$^+$ lifespan of ~ 7.6 years. Given the normal CD4$^+$:CD8$^+$ ratio of 2:1, the average combined naive T-cell clearance rate is $\mu_0 = \frac{1}{5.9}$ year^{-1} = 0.17 year^{-1}. Thymic involution within an aging human can be quantified by measuring the decrease in thymic epithelial volume (Steinmann 1986), based on which Murray et al. (2003) showed that thymic output decreases by an average of 4.3% per year between ages 0 and 100, implying a decay factor of $a = |\ln(0.957)| \simeq 0.044$. The rate of thymic export has recently been measured for young adults (20–25 years
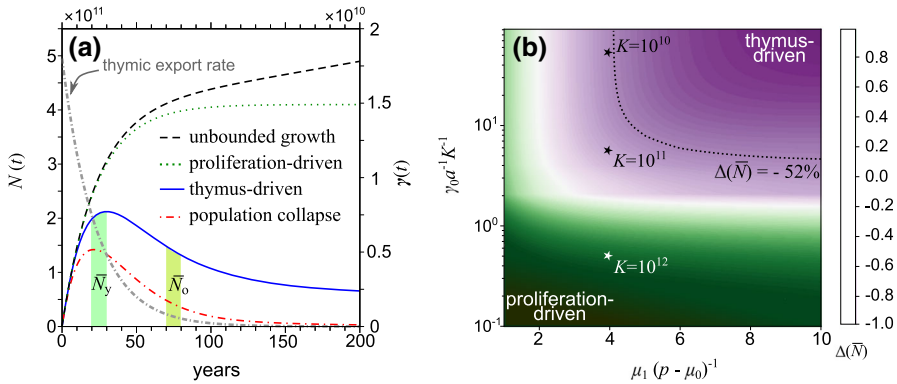
Fig. 1 (Color figure online) Qualitative behavior of the total naive T cell population model (Eqs. 1, 2). **a** The total naive T cell population $N(t)$ as a function of time (in years) for four qualitatively distinct scenarios. Unbounded growth arises when $\mu_1/(p - \mu_0) < 1$ and the naive T cell population collapses when $(p - \mu_0)/a < 0$. Outside of these two regimes, $N(t)$ converges asymptotically to a positive steady state as $\gamma(t) \to 0$. If $\gamma_0/(aK) \ll 1$, $N(t)$ is driven primarily by homeostatic proliferation and increases monotonically toward the constant plateau. Increasing $\gamma_0/(aK)$ leads to a transition from proliferation-driven scenario to thymus-driven populations, in which $N(t)$ reaches a peak value before converging to the steady state. The decaying thymic export rate $\gamma(t)$ is plotted alongside the $N(t)$ curves as a reference. To quantify the decrease in cell counts with age, we define $\bar{N}_y$ as the average of $N(t)$ between ages 20 and 30, and $\bar{N}_o$ between 70 and 80; then, $\Delta\left(\bar{N}\right) = \left(\bar{N}_o - \bar{N}_y\right)/\bar{N}_y$ is the relative change in cell counts. The parameter values used are $\gamma_0 = 1.8 \times 10^{10}$, $a = 0.044$, and $K = 10^{10}$ and $p = 0.022$, $\mu_0 = 0.017$, and $\mu_1 = 0.004$ for unbounded growth, $p = 0.17$, $\mu_0 = 0.18$, and $\mu_1 = 0.04$ for the collapse scenario, $p = 0.18$, $\mu_0 = 0.17$, and $\mu_1 = 0.01001$ for the homeostasis-driven case, and $p = 0.18$, $\mu_0 = 0.17$, and $\mu_1 = 0.04$ for the thymus-driven case. The initial value is $N(1) = 10^{10}$ at $t = 1$ year. **b** $\Delta\left(\bar{N}\right)$ as a function of $\gamma_0/(aK)$ and $\mu_1/(p - \mu_0)$. When $\gamma_0/(aK)$ and $\mu_1/(p - \mu_0)$ are small, $N(t)$ is driven primarily by proliferation and keeps increasing well into old age, leading to positive $\Delta(\bar{N})$ values. Conversely, for large $\gamma_0/(aK)$ and $\mu_1/(p - \mu_0)$, thymic export dominates and $N(t)$ peaks at early ages, resulting in negative $\Delta(\bar{N})$. The black dotted curve corresponds to $\Delta(\bar{N}) = -52\%$ as previously reported by Westera et al. for human adults. At fixed $\mu_1/(p - \mu_0) = 4$, we are able to reproduce this curve by setting $\gamma_0/(aK) \simeq 41$ (corresponding to $K = 10^{10}$ for our choice of parameter values). The value of $\Delta(\bar{N})$ increases with decreasing $\gamma_0/(aK)$ and becomes positive when $\gamma_0/(aK) \lesssim 1$. Here, we fixed $(p - \mu_0)/a = 0.2$ and $a = 0.044$

old) at $\sim 1.6 \times 10^7$ trained cells daily or equivalently 5.8×10^9 per year (Westera et al. 2015). Assuming that this rate is $\gamma(t)$ at $t = 25$ years, we can back-calculate $\gamma_0 = (5.8 \times 10^9) \times \left(\frac{100}{33.3}\right) \approx 1.75 \times 10^{10}$ cell exports/year. Note that these values of p, μ_0, and a satisfy the constraint $(p - \mu_0)/a > 0$ that prevents the human naive T-cell population from completely collapsing once $\gamma(t) \to 0$.

While direct experimental measurements of μ_1 and K are not available in the literature, further inspection of Fig. 1a reveals that μ_1 and K determine whether thymic export or homeostatic proliferation dominates the evolution of $N(t)$. Through the dimensionless parameters, $\gamma_0/(aK)$ and $\mu_1/(p - \mu_0)$, the time at which $N(t)$ peaks and how fast it declines from the peak vary with changes to the values of μ_1 and K. Recently, Westera et al. (2015) reported a 52% decrease in total naive T-cell counts between young human adults and elderly individuals, which we can use to quantitatively constrain μ_1 and K. Let us define individuals of an age between $t = 20$ and 30 years as young adults, and those between $t = 70$ and 80 as the elderly. Assuming

that interpersonal heterogeneity unrelated to age averages out over large sample sizes in clinical data, we may evaluate $\bar{N}_y = \frac{1}{10}\int_{20}^{30} N(t)\mathrm{d}t$ and $\bar{N}_\mathrm{o} = \frac{1}{10}\int_{70}^{80} N(t)\mathrm{d}t$ as the average naive T-cell counts, respectively, for the young and the elderly, as illustrated by the shaded areas under the thymus-domination curve in Fig. 1a. The relative change in the naive T-cell count between young and elderly adults can thus be evaluated as

$$\Delta(\bar{N}) = \frac{(\bar{N}_\mathrm{o} - \bar{N}_y)}{\bar{N}_y}. \tag{4}$$

Figure 1b plots $\Delta(\bar{N})$ as a function of $\gamma_0/(aK)$ and $\mu_1/(p - \mu_0)$, with $a = 0.044\ \mathrm{year}^{-1}$ for converting the dimensionless time to years to compute $\bar{N}_y$ and $\bar{N}_\mathrm{o}$. When $\gamma_0/(aK) \lesssim 1$ and $\mu_1/(p - \mu_0) \lesssim 2$, $\Delta(\bar{N}) > 0$. Note that the homeostatic carrying capacity when $\gamma(t) = 0$ is $N_\mathrm{ss}(\gamma = 0) = K(\mu_1/(p - \mu_0) - 1)^{-1}$. A small $\gamma_0/(aK)$ value represents a relatively low thymic export rate, and the carrying capacity increases rapidly as $\mu_1/(p - \mu_0) \to 1$, both of which make it challenging for thymic output to fill up the naive T-cell pool to carrying capacity before $\gamma(t)$ considerably decays within $t \sim a^{-1}$. As a result, $N(t)$ does not reach a peak value at a young age and continues increasing into old age. The $\approx 52\%$ decrease in naive T-cell counts reported by Westera et al. (2015) is depicted by the black dotted curve, which exhibits an abrupt turn around $\mu_1/(p - \mu_0) \approx 4$, suggesting that the value of $\mu_1/(p - \mu_0)$ may most likely be around or above four.

In "Appendix A," we further find that increasing $\mu_1/(p - \mu_0)$ leads to a higher fraction of the naive T cell population coming from direct thymic export. For $\mu_1/(p - \mu_0) \geq 10$, this fraction stays consistently above 25% throughout most of an adult human life, which exceeds previous experimental observations of 11–23% (den Braber et al. 2012), suggesting that 10 may be an upper bound on $\mu_1/(p - \mu_0)$. Without loss of generality, we set $\mu_1/(p - \mu_0) = 4$, yielding $K = 10^{10}$ by calibrating our model to reproduce this decrease in the cell count ($\gamma_0/(aK) \simeq 41$ with $\gamma_0 = 1.8 \times 10^{10}$ and $a = 0.044$). In contrast, $K = 10^{12}$ yields $\gamma_0/(aK) \simeq 0.41$, leading to an increase in the cell count ($\Delta(\bar{N}) \simeq 0.63$). In between, $K = 10^{11}$ results in a moderate decrease in the cell count ($\Delta(\bar{N}) \simeq -0.33$). For the rest of the paper, we fix $K = 10^{10}$ and $\mu_1/(p - \mu_0) = 4$, or equivalently $\mu_1 = 0.04$ given that $p = 0.18$ and $\mu_0 = 0.17$, so that the age-related decline of $N(t)$ in our model is consistent with Westera et al. (2015).

Note that there exist two intrinsic timescales in Eq. 1; thymic export decays at a rate a, while the homeostatic time scale is controlled primarily by p, μ_0, and also by μ_1 to a lesser degree. If homeostasis is much faster than thymic involution, the solution $N(t)$ will quickly converge to the quasisteady-state solution as $\gamma(t)$ evolves. We compare these two solutions in Fig. 2a, where the quasisteady-state solution is obtained by solving for the steady-state solution N_ss of Eq. 1 with fixed $\gamma(t)$ at each time t, and $N_\mathrm{ss}(\gamma(t))$ (black dashed curve) decreases monotonically with age due to the continuous decline of $\gamma(t)$. In contrast, $N(t)$ (blue solid curve) slowly rises from the initial condition $N(1) = 10^{11}$ and does not approach the quasisteady-state level until age ≈ 20 years. The trajectory of $N(t)$ then overshoots the declining $N_\mathrm{ss}(\gamma(t))$, reaches a peak value, and reverses course to go after $N_\mathrm{ss}(\gamma(t))$. However, $N(t)$ never catches up
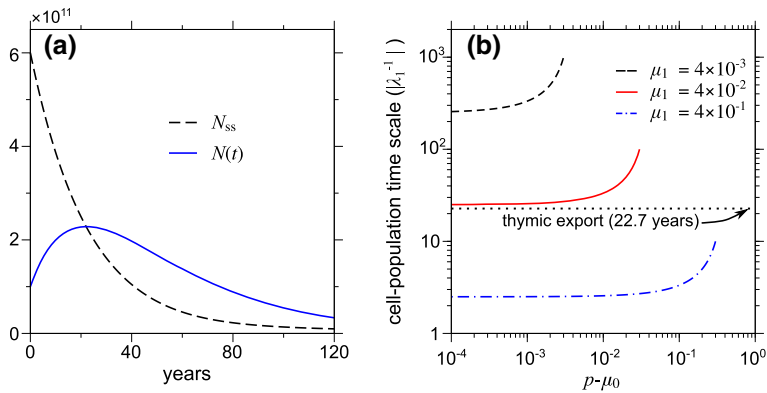
Fig. 2 (Color figure online) Comparison of thymic export and cell population evolution time scales. **a** Plots of $N(t)$ and N_{ss} show discrepancy. The $\gamma(t)$ dependence makes N_{ss} decline monotonically with the exponentially decaying thymic export, and N_{ss} approaches a small positive value as $\gamma(t) \to 0$. The solution $N(t)$ evolves toward N_{ss} but never catches up with it because of a slower evolution time scale. **b** Comparison of timescales of thymic atrophy and cell population evolution. Thymic atrophy is the faster mechanism for most choices of the system's parameters. Increasing μ_1 shortens the time scale of clone evolution, indicating that the steady-state solution can be a reasonable approximation to the fully time-dependent solution at very large μ_1 and very small $p - \mu_0$. Here, varying N_{ss} within the range $[10^{10}, 10^{12}]$ yields almost identical results, and the values of γ_0 and K, chosen within the reasonable parameter regime, do not affect the results significantly. Parameter values used are $\gamma_0 = 1.8 \times 10^{10}$, $a = 0.044$, $p = 0.18$, $\mu_0 = 0.17$, $K = 10^{10}$, $\Omega = 10^{16}$. In panel **a**, $\mu_1 = 0.04$, and the initial condition is $N(1) = 10^{11}$

with $N_{ss}(\gamma(t))$ before the latter reaches a steady state of very low cell counts. That $N(t)$ keeps lagging behind $N_{ss}(\gamma(t))$ indicates that the timescale for the full model solution to converge to the steady state is slower than the evolution of the nonautonomous term $\gamma(t)$. The results here suggest that steady-state solutions cannot adequately describe the temporal evolution of the naive T-cell population in the biologically relevant range of parameter values that we have implemented. It is necessary to numerically compute the time-dependent solutions for the full nonautonomous equation.

Indeed, we find a disparity in the rates at which thymic export decays and the steady-state solutions evolve. The latter is provided by the inverse of the eigenvalue of Eq. 1 linearized around $N = N_{ss}(\gamma(t))$. The eigenvalue takes the form $\lambda_1 = p_0 - (\mu_0 + \mu_1((3N_{ss}^2 K^2 + N_{ss}^4)/((K^2 + N_{ss}^2)^2)))$. Simulations in Fig. 2b show that for the biologically relevant parameter values we have implemented, the cell population evolution timescale, $|\lambda_1|^{-1}$ (red solid curve), is generally longer than the timescale of thymic involution ($a^{-1} \simeq 22.7$ years for $a = 0.044$ as denoted by the horizontal black dotted line). Hence, the nonautonomous solutions $N(t)$ are expected to lag behind the thymus-driven steady-state solutions N_{ss}. For $N(t)$ to be reasonably approximated by N_{ss}, the cell population has to evolve much faster than thymic involution, corresponding to the regime of very large μ_1, as indicated by the blue dashed–dotted curve, where cell death is extremely sensitive to the cell population size. However, μ_1 is bounded above by experimental observations, as discussed previously in parameter calibration. Thus, our conclusions derived from Fig. 2a and b should hold for parameter values within the biologically relevant range.

2.2 Clonotype Abundance Distributions

Quantification of the populations of individual clonotypes would require analysis of models that track the population dynamics of naive T-cells of each TCR type. Assuming the same population dynamics for each T-cell clonotype i, which may be appropriate in certain scenarios, the evolution of the expected cell count $n_i(t)$ may be deduced from Eq. 1 and take the following generalized form:

$$\frac{\mathrm{d}n_i}{\mathrm{d}t} = \frac{\gamma(t)}{\Omega} + pn_i - \mu(N)n_i, \tag{5}$$

where $\gamma(t)/\Omega$ represents thymic export of naive T-cells of *each* clonotype (the total thymic export rate normalized by the total number of viable TCR combinations Ω), and $N(t) = \sum_i n_i(t)$. Within the framework of these "neutral" models, basic qualitative behaviors of T-cell population dynamics have been investigated, particularly for scale-invariant properties that can be studied in a reduced system (Lythe et al. 2016; Desponds et al. 2015). Indeed, the total numbers of T-cell clonotypes Ω in rodent or human bodies are prohibitively large for direct numerical simulations of the full system using Eq. 5. It is thus common to reduce the full system to a more manageable size with the assumption that the phenomena under investigation are scale invariant. However, it is sometimes difficult to assert whether a certain property really does not change in a rescaled system, as nonlinear phenomena, such as the Allee effects, often arise in population dynamics and cast doubt on the scalability of the system. Moreover, some properties, such as the thymic export rate $\gamma(t)$, are naturally scale dependent. It is not always clear how these quantities should be rescaled in a reduced system, and they have usually been omitted by simplification arguments in previous models, which limits the applicability of these models.

In particular, thymic involution is known to be associated with the age-related loss of naive T-cell diversity. Without the explicit inclusion of the thymic export rate, such loss of naive T-cell diversity cannot be properly investigated. To facilitate a more manageable full-system model, we consider a formulation that tracks how the expected number of clones of a given size changes with time. By focusing on clone count rather than the explicit cell count of each distinct clonotype, we are able to effectively reduce the number of tracked variables and thus the dimension of the model. This representation was used by Ewens (1972) in population genetics, by Goyal et al. (2015) in the context of hematopoietic stem cell population dynamics, and by Desponds et al. (2017) in the context of T-cells. We define $\hat{c}_k(t)$ to be the number of clones represented by exactly k naive T-cells in the organism at time t:

$$\hat{c}_k(t) = \sum_{i=1}^{\Omega} \delta_{n_i(t),k}, \tag{6}$$

where the Kronecker delta function $\delta_{x,y} = 1$ when $x = y$ and 0 otherwise. By lumping clonotypes of the same cell count into one single variable $\hat{c}_k$, this alternative formulation can efficiently describe changes to the TCR clone diversity in the full system,

albeit at the expense of the ability to distinguish each specific clonotype (Morris et al. 2014; Mora and Walczak 2016). Individual clone information is lost, and $n_i(t)$ cannot be recovered from $\hat{c}_k(t)$ after the transformation in Eq. 6. Nonetheless, the amount of computation can be significantly reduced by truncating $\hat{c}_k(t)$ at a reasonably large k, as few large clones exist in realistic scenarios, and $\hat{c}_k(t)$ for large k is negligible. Letting $c_0(t) \equiv \langle \hat{c}_0(t) \rangle$ denote the expected number of all possible (thymus-allowed) clonotypes unrepresented in the periphery at time t, and $c_k(t) \equiv \langle \hat{c}_k(t) \rangle$ the expected number of clones of size k at time t, a set of equations governing the evolution of $c_k(t)$ consistent with Eq. 5 can be derived in the mean-field limit. Below, we provide a heuristic derivation and leave the more formal development to "Appendix B." The mean-field equation for the expected clone counts can be written as

$$\frac{dc_k(t)}{dt} = \frac{\gamma(t)}{\Omega} \left[c_{k-1} - c_k \right] + p \left[(k-1)c_{k-1} - kc_k \right] + \mu(N) \left[(k+1)c_{k+1} - kc_k \right],$$

(7)

where $N(t) = \sum_i^\infty n_i(t) = \sum_{\ell=1}^\infty \ell c_\ell(t)$. The expected values $c_k(t)$ are also called species abundances in the ecology literature. The number of unrepresented clones is $c_0 = \Omega - \sum_{k=1}^\infty c_k$, and summing Eq. 7 multiplied by k over $k = 1, 2, \ldots$ recovers Eq. 1. The mean-field assumption is articulated in terms such as $\mu(\sum_\ell \ell\hat{c}_\ell)\hat{c}_k$ that involve higher-order products of $\hat{c}_k$ rather than correlations of products of $\hat{c}_k$.

In Eq. 7, the terms in the forms of $(\gamma(t)/\Omega)c_k$, pkc_k, and $\mu(N)kc_k$ represent, respectively, the effect of thymic export, homeostatic proliferation and cell death on a naive T-cell clone already represented by k cells in the peripheral blood. Adding one cell via thymic export or homeostatic proliferation moves one clone from the c_k-compartment to the c_{k+1}-compartment, while the death of one cell shifts one clone from the c_k-compartment to the c_{k-1}-compartment. We approximate the proliferation rate, p, as a constant, at which rate all cells of all clones of size k replicate via homeostatic proliferation. Proliferation reduces c_k and increases c_{k+1}. Terms of the form $\mu(N)kc_k$, where the IL-7 regulated death rate $\mu(N)$ is given by Eq. 2, reduce c_k and increase c_{k-1}.

In a recent study, we found that the mean-field approximation breaks down only when $\gamma/\mu < 1/\Omega \ll 1$; under these circumstances, the total population is proliferation driven and the quasistatic configuration is $N \sim K$ and all $c_k \sim 0$ except c_N (Xu and Chou 2018). Thus, we reasonably assume that $\gamma(t) > \mu/\Omega$ allowing the use of the mean-field equations 7 in the rest of this paper.

For a healthy aging human adult, the naive TCR repertoire is mostly comprised of small clones with the probability of finding large clones decreasing with clone size k. To numerically solve Eq. 7, we thus truncate the model at a maximum clone size $M \gg 1$, beyond which the probability of finding a clone is assumed negligible. For our implementation of the truncation, please see "Appendix C." In Fig. 3a, we examine the effect of the truncation clone size M, showing sufficient convergence of c_{10} at $t = 40$ and 70 to fixed values when $M \gtrsim 30$, which indicates that further inclusion of clones beyond c_{30} has little effect on the solution for $t \lesssim 70$ years. For numerical simulations of Eq. 7 in this paper, we set $M = 200$ to ensure minimal truncation errors.
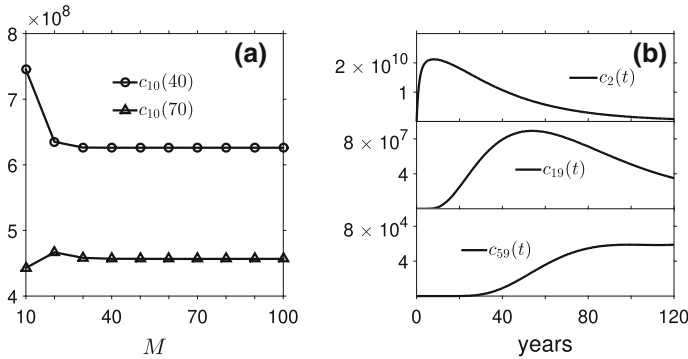
Fig. 3 Simulations of Eq. 7. **a** Effect of numerical truncation. We plot $c_{10}(40)$ and $c_{10}(70)$ as functions of M for $10 \leq M \leq 100$. Compartment sizes are effectively fixed when $M \gtrsim 30$. **b** Temporal evolution of $c_k(t)$. We plot $c_2(t)$, $c_{19}(t)$, and $c_{59}(t)$. Each $c_k(t)$ curve rises to a peak value and subsequently decreases. As k increases, $c_k(t)$ decreases in magnitude, and the time at which it reaches the peak value is pushed back. Parameter values: $\gamma_0 = 1.8 \times 10^{10}$, $a = 0.044$, $p = 0.18$, $\mu_0 = 0.17$, $\mu_1 = 0.04$, $K = 10^{10}$, $\Omega = 10^{16}$. Initial values $c_1(1) = 10^{11}$, $c_0(1) = \Omega - 10^{11}$, $c_k(1) = 0$ for all $k \geq 2$

Figure 3b shows the temporal evolution of $c_k(t)$ for $k = 2$, 19, and 59. As k increases, the overall magnitude of the $c_k(t)$ curve decreases, and the age at which $c_k(t)$ peaks increases. For example, $c_2(t)$ peaks around $t \lesssim 20$ years, and there are many fewer clones of exactly two cells in old age than at young ages. In contrast, $c_{19}(t)$ peaks around age 55, and the numbers of clones that have exactly 19 cells are roughly the same between old and young ages, whereas the number of clones that have exactly 59 cells ($c_{59}(t)$) keeps increasing into old age.

The relatively earlier decline of $c_k(t)$ with smaller k is expected, considering that rare clones are introduced into the peripheral circulation primarily by the thymus, which started to involute after birth. With increasing k, the influence of thymic export on $c_k(t)$ decreases, whereas the dependence on homeostatic proliferation increases. Recalling that the rate of thymic involution is faster than the time scale for homeostasis to drive the clonal population toward equilibrium, the fast decline of the rare clone population leaves room for larger clones to expand.

To accompany the steady state N_{ss}, we compute analogous fixed-γ_0 steady-state values of the full system, c_k^{ss}, in "Appendix D." The steady states satisfy $c_k^{ss} \to 0$ as $\gamma_0 \to 0$ for all $1 \leq k \leq M$. We further show that in spite of the fact that $c_k^{ss} \to 0$, Eq. 7 asymptotically yields a positive total cell count $N = \lim_{M \to \infty} \sum_{k=1}^{M} k c_k^{ss} > 0$ as $M \to \infty$, qualitatively consistent with Eq. 1. Moreover, we prove in "Appendix E" that solutions $c_k(t)$ of the full nonautonomous system satisfy $c_k(t) \to 0$ for all $k \leq M$, with arbitrarily large M, as $t \to \infty$. This result is completely independent of the assumed functional forms of the proliferation and death rates, suggesting that manipulation of homeostatic regulatory mechanisms cannot prevent the extinction of small T-cell clones caused by decaying $\gamma(t)$. We thus conclude that thymic involution dictates the age-related decline of the TCR diversity of the naive compartment.
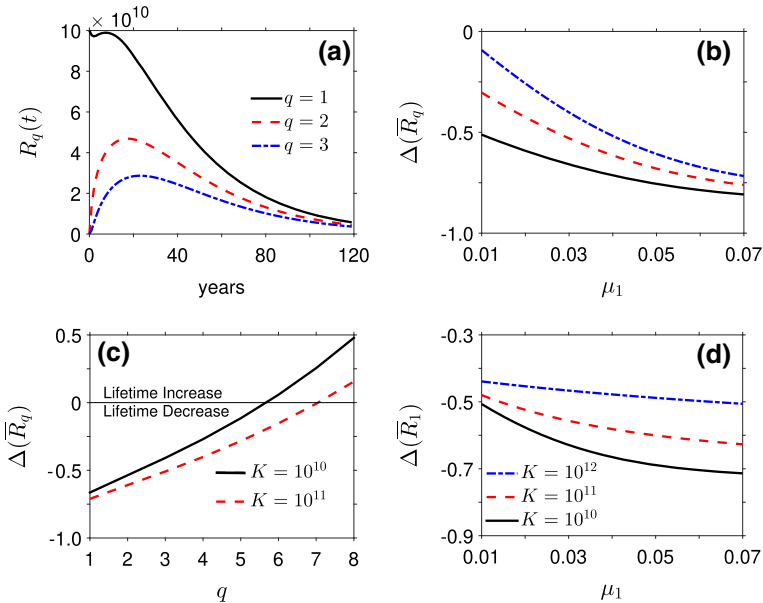
Fig. 4 (Color figure online) Simulation of threshold richness diversity. **a** $R_q(t)$ as a function of t, for $q = 1, 2, 3$. R_q peaks at later times as q increases. **b** $\Delta(\bar{R}_q(t))$ for varying q, μ_1. Higher μ_1 correspond to more severe loss of T-cell clones in advanced age. **c** $\Delta(\bar{R}_q)$ for varying q, K. Small values of q result in a lifetime decrease to R_q, but larger values result in a lifetime increase. This is due to the fact that R_q peaks at later times as q increases. **d** $\Delta(\bar{R}_1)$ for varying μ_1, K. Initial values $c_0(1) = \Omega - 10^{11}$, $c_1(1) = 10^{11}$ $c_k(1) = 0$ for $k \geq 2$. Parameter values, when not varying: $\Omega = 10^{16}$, $K = 10^{10}$, $p_0 = 0.18$, $\mu_0 = 0.17$, $\mu_1 = 0.04$, $a = 0.044$, $\gamma_0 = 1.8 \times 10^{10}$

2.3 Diversity of the Naive T-cell Repertoire

By computing the functions c_k that track the number of clones consisting of k cells, we should have sufficient information to evaluate the variation in naive TCR structural diversity over a lifetime. Expected naive TCR structural diversity or "richness" is the total number of distinct naive T cell clones present in the immune compartment, for which we define a threshold naive TCR richness diversity

$$R_q(t) = \sum_{k \geq q} c_k(t), \tag{8}$$

where $q \in \mathbb{N}$ is a threshold, so that the quantity $R_q(t)$ represents the number of clones of size at least q present in the immune compartment at time t. $R_q(t)$ is a generalization of $R_1(t)$, which is typically defined as the richness of naive TCR diversity. A higher threshold $q > 1$ may arise because of immune surveillance, in which small clones may evade detection, or effectiveness of antigen detection, in which small clones may have an insufficient probability of encountering their specific antigens.

As shown in Fig. 4a, $R_q(t)$ increases at young ages, peaks at a mature age, and declines afterward. For our previous parameter values, the peak age of $R_1(t)$ is approx-

imately $t \sim 16$. Higher q leads to older peak ages of $R_q(t)$, consistent with the results in Fig. 3b, in which the number of larger clones peaks in old age.

To compare $R_q(t)$ between the elderly and young, we adopt the same criterion as with total cell counts and compute window-averaged values of $R_q(t)$ between ages 20 and 30 for the young and between ages 70 and 80 for the elderly. By defining $\bar{R}_y(q) \equiv \frac{1}{10} \int_{20}^{30} R_q(t) \mathrm{d}t$, $\bar{R}_o(q) \equiv \frac{1}{10} \int_{70}^{80} R_q(t) \mathrm{d}t$, we quantify the loss of richness by computing its relative change:

$$\Delta(\bar{R}_q) \equiv \frac{(\bar{R}_o(q) - \bar{R}_y(q))}{\bar{R}_y(q)}. \tag{9}$$

Using the same parameter values as shown in Fig. 4a, we plot $\Delta(\bar{R}_q)$ with respect to μ_1 and q in Fig. 4b and c. In Fig. 4b, $\Delta(\bar{R}_q)$ decreases monotonically with increasing μ_1, suggesting that upregulated death rate exacerbates the age-related loss of richness, and the impact is more significant for larger q. Figure 4c shows that when $K = 10^{10}$, $\Delta(\bar{R}_q) < 0$ for $q \leq 4$. This decreasing trend of R_q generally agrees with the loss of diversity observed in recent experiments where measurements were available across multiple ages (Qi et al. 2014; Britanova et al. 2014). For $q = 5, 6$, $\Delta(\bar{R}_q) \approx 0$, and R_q is nearly unchanged between youth and advanced age. For $q \geq 7$, $\Delta(\bar{R}_q) > 0$, indicating higher R_q in old age. Generally, the lifetime decrease in $R_q(t)$ occurs with small q, whereas for large q, the trend is reversed, in agreement with our discussion of Figs. 3b and 4a regarding peak ages. This phenomenon indicates that loss of diversity is primarily due to the extinction of rare clones, which is consistent with the observation made by Naylor et al. (2005). In contrast, the number of larger clones increases over time, leading to the lifetime increase to $R_q(t)$ at higher q.

Recent TCR-β sequencing studies have attempted to estimate the change in the repertoire richness of the naive T-cells with age. Despite the difference in orders of magnitude regarding the total number of circulating naive T-cell clones, these studies agreed quantitatively in the ratio of the age-related loss of richness. For example, Britanova et al. (2014) estimated $\sim 7 \times 10^6$ clonotypes in youth (ages 6–25) and $\sim 2.4 \times 10^6$ in aged individuals (ages 61–66), a roughly 66% drop from the youth figure. Similar measurements were also reported by Qi et al. (2014), in which a two- to fivefold decline (i.e., a 50–80% drop) between youth (ages 20–35) and advanced age (ages 70–84) was observed. These results are quantitatively consistent with our computation of $\Delta(\bar{R}_1)$ for $K = 10^{10}$–$10^{11.5}$ and $0.03 \leq \mu_1 \leq 0.05$ in Fig. 4d, whereas the decline of R_q for $q \geq 2$ is not as pronounced as in these experimental observations.

Also note that the loss of clonal richness is more severe than the decrease in the total cell count between young and aged individuals. In Fig. 4a, $\Delta(\bar{R}_1)$ changes between $\sim -66\%$ and $\sim -76\%$ for $0.03 \leq \mu_1 \leq 0.05$ and $K = 10^{10}$. In contrast, Fig. 1b shows that for the same parameter range, $\Delta(\bar{N})$ varies from $\sim -30\%$ to $\sim -62\%$. However, the figures also reveal that richness is relatively less sensitive to changes to the cellular death rate, compared to the total cell count. This outcome reflects the fact that homeostatic cellular death is uniformly random across the entire naive T-cell population. The drop in richness is due to cell death within small clones that drives these clones to extinction, as observed by Naylor et al. (2005). Increases to

the cellular death rate do not cause as much additional clonal extinction as they do additional cellular extinction, as many surviving clones are too large to wipe out by the death of a few cells.

2.4 Sampling Statistics

Considering that naive T-cell richness is often assessed via small blood samples, let us next use the same framework to examine the relation between the detected clone sizes in small samples and the true clone sizes in the full organism. As before, denote by N the total number of naive T-cells in the human's immune compartment and $Y \leq N$ the number of cells collected during sampling from among the N total. We assume that the N total cells consist of R distinct clones, which we number from 1 to R. In this section, we denote by c_k^N the mean number of clones of size k from among the N total cells in the full organism (denoted by c_k in the previous simulations) and by c_k^Y the mean number of clones of size k in the sampling of Y cells taken from the N total cells. Then the expectation of c_k^Y, denoted by $\mathbb{E}[c_k^Y]$, is:

$$\mathbb{E}\left[c_k^Y\right] = \sum_{j=1}^{R} j P \left(c_k^Y = j\right), \tag{10}$$

where $P\left(c_k^Y = j\right)$ represents the probability that there are precisely j clones of size k in the sampling. Then $\mathbb{E}[c_k^Y]$ may be expressed explicitly in terms of the c_k^N as:

$$\mathbb{E}\left[c_k^Y\right] = \sum_{l=k}^{R} \frac{1}{\binom{N}{Y}} c_l^N \binom{l}{k} \binom{N-l}{Y-k}. \tag{11}$$

(See "Appendix F" for the detailed proof.) The collection of expressions given by Eq. 11 for $k = 1, 2, \ldots, R$ yields a linear system of equations solvable for c_k^N, using sampled data for the quantities $\mathbb{E}[c_k^Y]$. More specifically, if we define the vectors $\widehat{\mathbf{E}} := (\mathbb{E}[c_1^Y], \mathbb{E}[c_2^Y], \ldots, \mathbb{E}[c_R^Y],)$ and $\mathbf{E} := (c_1^N, c_2^N, \ldots, c_R^N)$, Eq. 11 can be written as $\widehat{\mathbf{E}} = \mathbf{AE}$, where $\mathbf{A}$ is a constant matrix that has nonzero elements only in the upper triangle, with nonzero diagonal entry $\frac{1}{\binom{N}{Y}}\binom{N-k}{Y-k}$ in position (k, k). The equation can always be solved uniquely for $\mathbf{E}$ given $\widehat{\mathbf{E}}$. Thus, the full size distribution $\mathbf{E}$ can be uniquely reconstructed from the expected mean sample size distribution $\widehat{\mathbf{E}}$ measured experimentally, provided that the latter can be reliably estimated through a sufficient number of repeated samplings.

In Fig. 5a, we use Eq. 11 to compute $\mathbb{E}[c_k^Y]$ from simulated c_k^N, comparing the predicted sampling results of the richness $R_1(t)$ for varying choices of Y. The results indicate that each decrease by one order of magnitude to the sample size results in a decrease in $R_1(t)$ by roughly the same order of magnitude to the predicted diversity, except between the full sample and one-tenth of the sample ($f = 10^{-1}$), where the decrease in $R_1(t)$ is less than one order of magnitude. Predictions of diversity vary with sample size, and small samples do not result in accurate measurements of diversity.
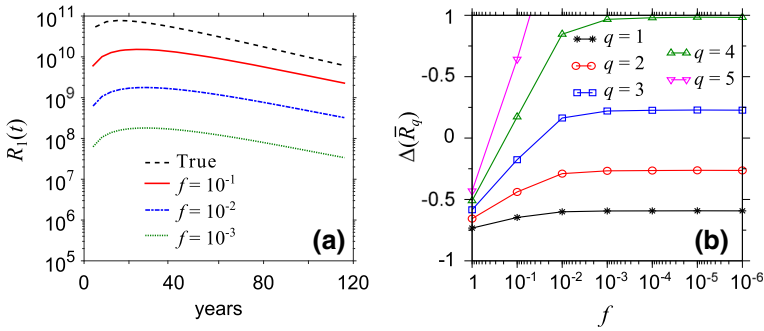
Fig. 5 (Color figure online) Comparison of actual and sampled richness. **a** True lifetime R_1, as well as the expected R_1 that result from extracting 10%, 1%, and 0.1% of the total cell count for sampling. ($Y = f \times N$, with $f = 10^{-1}, 10^{-2}, 10^{-3}$.) Except between the full sample and $f = 10^{-1}$, each decrease in the sample size by one order of magnitude results in a decrease to the expected R_1 by approximately one order of magnitude. **b** The ratio of age-related TCR richness decline $\Delta \left(\bar{R}_q \right)$ as a function of sampling fraction f for clone size thresholds $q = 1$–5. As f decreases, the value of $\Delta \left(\bar{R}_q \right)$ increases, indicating a lower estimate of the TCR richness decline. When f is very small, $\Delta \left(\bar{R}_q \right)$ becomes insensitive to further decreases to f. Parameter values used: $\gamma_0 = 1.8 \times 10^{10}$, $a = 0.044$, $p = 0.18$, $\mu_0 = 0.17$, $K_0 = 10^{10}$, $\Omega = 10^{16}$, $\mu_1 = 0.04$. Initial values $c_0(0) = \Omega$, $c_k(0) = 0$ for $k \geq 1$

In Fig. 5b, we examine how sampling may affect the diagnosis of the age-related TCR richness decline $\Delta \left(\bar{R}_q \right)$ defined in the previous subsection. We find $\Delta \left(\bar{R}_q \right)$, which is negative, increasing with decreasing sampling fraction f, revealing that sampling causes an underestimate of the richness decline. As previously discussed, the decline of TCR richness in old age is primarily due to the extinction of small clones. Since small clones often evade detection during sampling, their extinction is largely unaccounted for, leading to lessened reduction in the richness measure. When f is very small, most of the small clones have escaped detection; thus, decreasing f further does not change $\Delta \left(\bar{R}_q \right)$. Moreover, we note that $\Delta \left(\bar{R}_1 \right)$, which represents the case in Fig. 5a and is the most straightforward measure for age-related loss of TCR richness, converges from -73% for the full sample, to -59% for a sampling fraction $f \lesssim 10^{-2}$, which is close to the value of $\Delta \left(\bar{R}_3 \right)$ for the full sample. This reaffirms our discussion in the previous subsection that a threshold $q > 1$ may arise during the process of sampling. The results here indicate that when only a small fraction of a T-cell population is used to measure $\Delta \left(\bar{R}_1 \right)$, clones fewer than three cells largely evade detection, yielding a result equivalent to $\Delta \left(\bar{R}_3 \right)$ of the full sample, which underestimates the actual decrease in the TCR richness. Also note that the convergence of $\Delta \left(\bar{R}_1 \right)$ for $f \lesssim 10^{-2}$ corresponds to the proportional downscaling of $R_1(t)$ in Fig. 5a with decreasing f. For larger q, $\Delta \left(\bar{R}_q \right)$ does not converge until f is lower, indicating that $R_q(t)$ does not downscale proportionally until the sample fraction is very small.

3 Discussion

We have formulated a model of lifetime human naive T cell population dynamics, which traces T cell lineages on the level of individual clones. It accounts for expo-

nentially decaying lifetime thymic export, a constant rate of cellular proliferation, and variable cellular death rate that adjusts to present cell counts and the availability of survival resources. It depicts the generation of the naive T cell pool in early life via thymic export, and long-term maintenance of the population via peripheral turnover after thymic export has waned. Values of most of the model's parameters can be found in the previous literature on humans, while the few exceptions are obtained by fitting some basic results of the model, such as age-related T cell loss, to experimental observations. Our analysis serves two important purposes: to map the thymic machinery, identifying which components do and do not contribute to age-related cellular loss, and then to interpret the nuanced role of that cellular loss in immunosenescence. While our results are intended for describing human aging, our approach can be adapted and interpreted to mice where thymic output plays a larger role in sustaining the naive T cell pool and where we might expect the diversity to be more immediately sensitive to changes in thymic output rates. In either case, we have found that if thymic export is assumed to decay exponentially to zero, then all compartments $c_k(t)$ (with $1 \leq k \leq M$) deplete as $t \to \infty$, independent of essentially any restrictive assumptions about the homeostatic proliferative mechanism in the periphery. Concretely, for any choice of proliferation and death rates $p(N), \mu(N)$, that satisfy $p(0), \mu(0) > 0$ and the choice $\gamma(t) = \gamma_0 e^{-at}$ with $\gamma_0, a > 0$, there exists a sufficiently small $\delta > 0$ guaranteeing $c_k(t) \to 0$ as $t \to \infty$ for all $1 \leq k \leq M$, provided that $\sum |c_k(1)| \leq \delta$. Although this result only guarantees that trajectories $c_k(t)$ started sufficiently close to zero converge to zero, simulation indicates that the basin of attraction to this "zero state" is actually quite large. In fact, for the typical initial conditions used throughout this paper, simulation suggests convergence of all compartments c_k to zero in infinite time.

Although it takes an extremely long time to deplete all c_k compartments for $1 \leq k \leq M$, the initial phase of this process can still cause significant loss of T cell diversity in aging individuals within a human lifespan. Most importantly, we find that the T cell loss driven by exponentially diminishing thymic export *alone* is robust against any assumptions about the homeostatic proliferative mechanism in the periphery that depend uniformly on the population size N, as this outcome is universal for all functional forms of $p(N), \mu(N)$. Even a particularly strong homeostatic mechanism (say, one with $p(0) \gg \mu(0)$) cannot rescue a plunging diversity. This, in turn, suggests that in searching for treatments of age-induced loss of diversity, efforts should be directed at the thymus, in particular to maintaining thymic productivity into advanced age. In reality, heterogeneity can arise in the rates of peripheral proliferation and thymic output for naive T cells of distinct TCR expressions, due to differentiated responses to various growth factors in the periphery (Desponds et al. 2015; Lythe et al. 2016) and disparate sequencing frequencies in the thymus (Marcou et al. 2018). Even for naive T cells of identical TCR expressions, the peripheral proliferation rate decreases due to telomere shortening with each cell division (Weng et al. 1995; Hodes et al. 2002). Heterogeneity among different TCR expressions may provide a fitness advantage for certain clones and allow them to survive relatively longer than others when the TCR diversity is plunging. Telomere shortening likely makes older clones more easily replaced by newer ones, increasing the turnover rate of distinct TCR clones. Nevertheless, we do not expect such heterogeneity to qualitatively change our results here and rescue the diminishing TCR diversity caused by thymic involution.

Moreover, we compare the real-time simulations and the quasisteady-state solutions of the total cell count, as well as the number of distinct clones, over the course of age-related thymic output erosion. We find that our simulation results keep lagging behind the quasi steady-state solutions, suggesting that the erosion time scale of thymic output is faster than the time scale for the population dynamics to relax toward a steady state. Mathematically, this result reveals that the evolution of the T cell population within the human lifespan is a rather dynamical phenomenon, which may not be well described by quasistatic solutions, requiring evaluation of the fully nonautonomous system. Biologically, our results indicate that the loss of T cell diversity is a delayed response to thymic involution, and assessment of thymic function may predict the health of the immune system.

Although peripheral division cannot salvage the T cell population on a long time scale, higher basal proliferation rates may at least delay the erosion of the T cell compartment, sustaining acceptable effectiveness of the immune system within the human lifespan (Naylor et al. 2005). We assumed a constant lifetime rate of cellular proliferation, but alternative research suggests that proliferation rates may increase with age (Naylor et al. 2005). In light of this finding, we briefly inspect the effect of increased proliferation rates at advanced ages on cellular and clonal loss by modifying $p(N)$ and $\mu(N)$ in Eq. 7. To prevent unbounded growth caused by $p(N)$ exceeding $\mu(N)$ as $N \to +\infty$, we adopt a logistic growth rate, $p(N, t) = p(t)(1 - N/K)$, where growth is bounded by the negative term; a discrete increase in the proliferation rate is incorporated in $p(t) = p_0(1 + rH(t - T))$, with $p_0 > 0$ the early-life basal cellular proliferation rate, and $H(t)$ the Heaviside function, with T the age at which the rate increases. The constant r specifies the increase to the proliferation rate. The death rate is set to a constant value ($\mu(N) = \mu_0 > 0$) for simplicity, omitting the N-dependent term in Eq. 2 that practically becomes negligible compared to the negative term of $p(N)$ as $N \to +\infty$. By varying r, simulation under these alternate hypotheses indicates that increased basal proliferation rates do lead to notably higher total cell counts (Fig. 6a), but have little effect on diversity (Fig. 6b). These results further affirm that expansion of peripheral proliferation is unlikely to rescue the eroding naive T cell diversity, despite the increased cell count. If diversity loss is the main cause of immunosenescence (still a debatable topic in the medical community), peripheral proliferation may not be the sensible target of treatments.

The increased $N(70)$ and nearly unchanged $R_1(70)$ in Fig. 6 imply that the decline of T cell diversity in old age may appear more dramatic if the diversity is measured in terms of the frequency of distinct TCR sequences among the cycling cells, which corroborates the explanation that an increase in the proliferation rate in old age leads to a sharp decrease in T cell diversity (Naylor et al. 2005). Previous models have shown that even sharper decline of T cell diversity can be induced by fitness selection, where certain clonotypes increase their fitness in old age possibly due to higher avidity to self-antigens (Johnson et al. 2012, 2014; Goronzy et al. 2015a).

Although the boosts to the total cell count through artificial expansion of the proliferative mechanism are unable to replenish the declining TCR diversity in the naive T cell pool, it is possible that the impact is less severe than the decaying richness would have indicated, considering that most of the extinct clones are originally small clones, which may be much less effective than larger clones. In this regard, the viability of
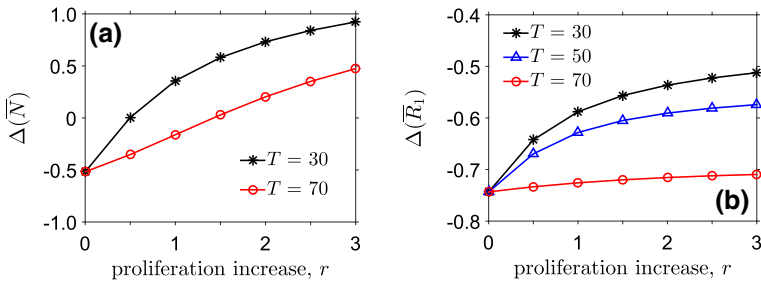
Fig. 6 (Color figure online) Total cell count and richness with rise in proliferation. Simulation of Eq. 7 with exponentially decaying thymic export, and peripheral homeostasis described by time-varying logistic growth. We use the thymic export rate $\gamma(t) = \gamma_0 e^{-at}$, peripheral death rate $\mu(N) = \mu_0 > 0$, and peripheral proliferation rate $p(N, t) = p(t)(1 - (N/K))$, with $p(t) = p_0(1 + rH(t - T))$. Here, $H(t)$ represents the Heaviside function with jump at $t = 0$. The constant r determines the magnitude of the increase to the basal proliferation rate, and T represents the time at which the jump occurs. We take the jump to occur at varying ages. **a** $\Delta(\bar{N})$ with jump at ages $T = 30$ and 70, for varying r. (Curve corresponding to $T = 50$ is omitted due to close similarity to $T = 30$ curve.) Raising the basal proliferation rate diminishes cellular loss in advanced age, with sufficiently high values of r producing a lifetime increase in total cell counts. The positive steady-state solution of the autonomous total cell ODE, $dN/dt = \gamma_0 + p_0(1 - N/K) - \mu_0 N$, is given by $N^* = (K/2)(1 - \mu_0/p_0 + \sqrt{(1 - \mu_0/p_0)^2 + 4\gamma_0/Kp_0})$ and can be seen to satisfy $\partial N^*/\partial p_0 > 0$ if $\gamma_0 < K\mu_0$, suggesting that increases to the basal proliferation rate are likely to increase the total cell count. **b** $\Delta(\bar{R}_1)$ with $T = 30$, 50, and 70, for varying r. Increases to the basal proliferation rate do mitigate diversity loss, but the effect is minor and potentially insignificant. Increases to the basal proliferation rate increase c_{k+1} due to a decrease in c_k, preserving additional diversity, but the lifetime diversity loss is still observed, even when proliferation rates are high enough to generate a lifetime increase to the total cell count. Fixed parameter values: $\gamma_0 = 1.8 \times 10^{10}$, $a = 0.044$, $p_0 = 0.18$, $\mu_0 = 0.17$, $K_0 = 3 \times 10^{11}$, $\Omega = 10^{16}$. Initial values: $c_0(1) = \Omega - 10^{11}$, $c_1(1) = 10^{11}$ $c_k(1) = 0$ for $k \geq 1$. Equation 7 is truncated at $k = 200$

treating immunosenescence by expanding peripheral proliferation depends on the elucidation of the T cell pool's *effectiveness clone size*—that is, the size a clone must have attained to effectively guarantee activation of the clone when its cognate antigen infiltrates the organism. The effectiveness clone size is intrinsically linked to true functional TCR diversity; if we can identify a threshold integer q^*, such that clones of size at least q^* are reliably activated in the presence of their cognate antigen(s), but that smaller clones are not, then $R_{q^*}(t)$ is naturally the most useful measure of diversity, because it accounts for precisely those clones actively participating in the adaptive immune mechanism. The larger the "correct" choice of q^* is, the more effective treatments to boost cellular proliferation in the periphery will be. Our model directly yields the number of clones of a particular size, making it straightforward to include or exclude clones below a certain cell count, should such a threshold exist and be identified.

The effectiveness clone size is also significant to the question of whether diversity loss is the driving factor in immunosenescence. Using the parameter values that we found in the literature, $R_q(t)$ decreases for $q \leq 4$ from youth to advanced age, stays nearly constant for $q = 5, 6$, and increases for $q \geq 7$. The extinction of small clones allows the surviving clones to expand in size, leading the richness of large clones to increase in old age. If the minimal size for a T cell clone to effectively respond to antigens is large, the diversity of such "effective" clones may actually increase with

age, strengthening the immune response. Therefore, either the minimal clone size required for effective immune response is low, or the weakened immune response in old age is caused primarily by other mechanisms. For example, functional deficiencies acquired by naive T cells in aging are one possible alternative cause of the weakened immune response. Such functional deficiencies have been studied heavily in mouse models, but research in humans is still lacking (Appay and Sauce 2014). Diminished naive T cell effector responsiveness and proliferative capacity have been observed in aged mice (Moro-García et al. 2013). It is possible that similar changes occur in humans. Conversely, experiments on mice have directly shown that loss of TCR diversity does have an actively detrimental effect on immune responsiveness (Yagger et al. 2008), supporting the notion that loss of TCR diversity is a significant contributor to immunosenescence.

Our model illustrates the feasibility of several different scenarios, in which loss of naive T cell diversity contributes to immunosenescence on drastically different levels. While we consider only the naive T cell population, memory T cells expand upon encountering antigens over the lifespan of an individual, eventually outnumbering naive T cells at around 30–40 years of age (Saule et al. 2005). Memory T cells rely on a mixture of IL-7 and IL-15 as survival signals (Rubinstein et al. 2008), which may reduce the amount of IL-7 available to naive T cells. However, memory T cells are observed to down-regulate expression of IL-7 receptor CD127 when the local concentration of IL-7 is low, thus preserving the naive repertoire (Surh and Sprent 2008). In addition, distinct population dynamics have been observed among various subsets of memory T cells, such as $CD4^+/CD8^+$ central memory/effector memory/terminally differentiated T cells (Saule et al. 2005), as well as among memory T cells expressing naive phenotypes that accumulate with aging but do not contribute to the capacity to respond to new infections (Pulko et al. 2016). While a more complete picture of T cell population dynamics would include the memory compartment, our model may serve as a first step in that direction, in which each subset of memory T cells may be added. Moreover, our model indicates that the effectiveness clone size and crossreactivity *in vivo* are valuable pieces of missing information, the elucidation of which would allow for the identification of effective options to treat immunosenescence.

4 Summary and Conclusions

We have simulated the time evolution of the functions $c_k(t)$, which represent the number of naive T cell clones of size k present in a human's immune compartment at time t. We determined that under essentially any realistic assumptions about homeostatic proliferation and death, all clones deplete in infinite time if thymic export is assumed to decay exponentially. This implicates thymic export as a fundamental cause of age-associated diversity loss. We simulated our model under the assumption that a carrying capacity is regulated by homeostatic proliferation and death through N-dependent rates. We found that the manipulation of homeostatic proliferation and death rates, which may notably raise the carrying capacity and thus the total cell count, was unable to save falling diversity as an individual ages. It affirms the vital role of thymic output in age-related diversity loss and indicates that boosting the pro-

liferation rate is unlikely an effective solution. However, if only clones of large size are sufficiently effective in the immune response, boosting proliferation rates might raise average clone sizes and help to mitigate the effects of lost diversity. We simulated "threshold richness diversity," $R_q(t)$, which counts the total number of clones of size q or larger. We found that by increasing q, the trajectory of $R_q(t)$ changes from decreasing to increasing over a human lifetime. From this trend, we concluded that if only large clones are effective, the effective richness would actually increase with age, suggesting that it is important to identify the minimal effective clone size in order to determine whether the loss of TCR diversity is the primary driving mechanism of the immune dysfunction seen in advanced age. Lastly, we derived a one-to-one mapping between the full-sample diversity c_k^N of N cells and the expected measurement of diversity $\mathbb{E}[c_k^Y]$ in samples of Y cells. We found that the probability of detecting small clones shrank significantly with small sample sizes, which could potentially skew small sample statistics. In particular, we show that small samples tend to underestimate the age-related loss of T cell richness diversity. Our formulation provides a rigorous method for accurately inferring the statistical distribution of clonal sizes from small sample measurements.

A Thymic Export and Proliferation Subpopulations

While the total cell count, N, of the naive T cell population is governed by Eq. 1 in our model, the subpopulation directly exported from the thymus N_{thy} can be explicitly tracked via

$$\frac{dN_{\text{thy}}(t)}{dt} = \gamma(t) - \mu(N)N_{\text{thy}}(t). \tag{A1}$$

The subpopulation of proliferation-generated cells is thus $N - N_{\text{thy}}$, assuming for simplicity that the cell death rate depends only on the total population and is the same for both subpopulations. Equation A1 allows us to determine whether the majority of the naive T cells are directly exported from the thymus or generated by peripheral proliferation.

The evolution of $N(t)$ and $N_{\text{thy}}(t)$ is shown in Fig. 7a and b for proliferation-driven, thymus-driven, and population collapse scenarios. The proliferation-driven and the thymus-driven scenarios are identical to the corresponding cases shown in Fig. 1a; for both cases, only a small fraction of the total naive T cell population is directly exported by thymus with the majority generated by peripheral proliferation. This limit is consistent with what was previously found for human naive T cell populations (den Braber et al. 2012). For the scenario of population collapse in Fig. 7c, naive T cells directly exported from the thymus comprise the majority of the naive T cell population, consistent with naive T cells in mice (den Braber et al. 2012). For this case, we adopt the same parameter values as in the corresponding case in Fig. 1a, but change μ_0 to
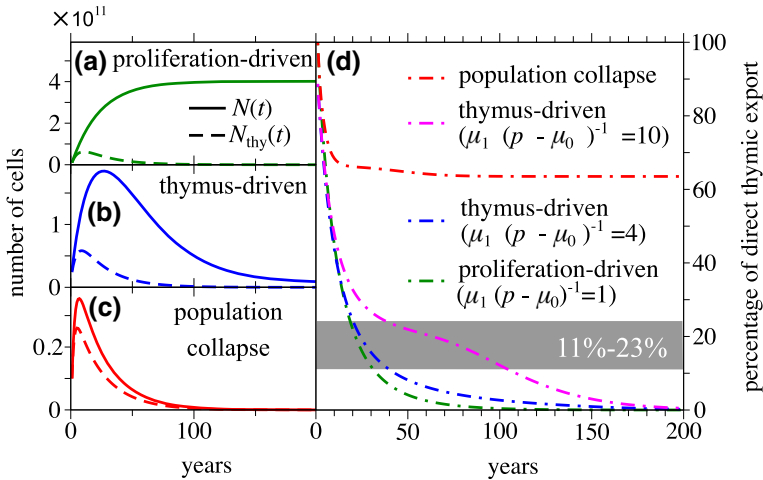
Fig. 7 (Color figure online) Thymus-produced vs. proliferation-generated subpopulations. **a–c** show the number of total cells $N(t)$ and the number of cells directly exported from the thymus $N_{thy}(t)$ for proliferation-driven, thymus-driven, and population collapse scenarios, respectively. Parameter values used are the same as those for corresponding curves in Fig. 1a, except that μ_0 is set to 0.51 in **c** so that the death rate is more than three times higher than the proliferation rate, as reported for naive T cells in mice. The initial conditions are also the same as those in Fig. 1a, whereas all cells are assumed exported from the thymus initially. The fractions $N_{thy}(t)/N(t)$ are plotted in **d** for these three scenarios, with an additional thymus-driven case in which $\mu_1/(p - \mu_0) = 10$. The shaded region highlights the 11–23% fraction of direct thymic export reported for naive T cells in human adults (den Braber et al. 2012)

0.51, as previous experiments find that in mice, the cell division time is about three to 14 times longer than the average cell lifespan (den Braber et al. 2012), implying that the cell death rate is about three to 14 times faster than the cell proliferation rate. Note that as $t \to \infty$ and $\gamma(t) \to 0$, both $N_{thy}(t)$ and $N(t) \to 0$ for the scenario of population collapse, while for thymus-driven and proliferation-driven cases, only $N_{thy}(t) \to 0$ and $N(t)$ converges to a nonzero steady state. This distinction is quantitatively illustrated by the time evolution of the fraction $N_{thy}(t)/N(t)$ in Fig. 7d. Initially all naive T cells are directly exported from the thymus; the percentage decreases over time, plateaus around 65% in the case of population collapse, and approaches zero in the thymus-driven and proliferation-driven cases. Previous studies find that in human adults 11–23% of the total naive T cell population is directly exported from the thymus, and we highlight this range of percentages by the shaded area. We find that for the thymus-driven case shown in Fig. 7b, where the parameter $\mu_1/(p - \mu_0) = 4$, this percentage range corresponds to ages from ~ 20 years to almost 50 years. In contrast, for the proliferation-driven case, where $\mu_1/(p - \mu_0) = 1$, this percentage range corresponds to a narrower age range (~ 20–30 years), implying that the fraction $N_{thy}(t)/N(t)$ may be dropping too fast and is below the experimental observation for most of adult life. Additionally, we examine another thymus-driven case with $\mu_1/(p - \mu_0) = 10$ in which the fraction $N_{thy}(t)/N(t)$ decreases slowly and stays above the experimental observation for most of adult life. Therefore, we conclude that

the parameter $\mu_1/(p - \mu_0)$ should be bounded between one and ten, motivating our choice of $\mu_1/(p - \mu_0) = 4$.

B Derivation of the Equation for Mean Clone Counts $c_k(t)$

If we formally define $P(n_1, n_2, \ldots, n_\Omega, t)$ as the probability of observing n_1 cells of clonotype 1, n_2 cells of clonotype 2, and so on, the average over the definition in Eq. 6, $\hat{c}_k(t) \equiv \sum_{i=1} \delta_{n_i(t),k}$ can be formally written as $c_k(t) \equiv \langle \hat{c}_k(t) \rangle = \Omega P(n = k, t)$ where $P(n, t) \equiv \sum_{n_2=0}^{\infty} \cdots \sum_{n_\Omega=0}^{\infty} P(n_1, n_2, \ldots, n_\Omega, t)$ is the single-clone marginal probability. This single-clone probability obeys a simple birth–death–immigration master equation

$$\frac{dP(k, t)}{dt} = \frac{\gamma(t)}{\Omega} [P(k-1) - P(k)] + p[(k-1)P(k-1) - kP(k)]$$
$$+ \mu(N)[(k+1)P(k+1) - kP(k)], \tag{A2}$$

where N is the total population that includes the population K of the singled-out clone. Thus, to close Eq. A2, a model for the stochastic dynamics of N is required. A mean-field model can be implemented by approximating the stochastic variable N by the deterministic solution $N(t)$ found by solving Eq. 1. The mean-field approximation thus neglects the correlation between the clone population k and the total population N, leading to Eq. 7

$$\frac{dc_k(t)}{dt} = \frac{\gamma(t)}{\Omega} [c_{k-1} - c_k] + p[(k-1)c_{k-1} - kc_k] + \mu(N(t))[(k+1)c_{k+1} - kc_k]. \tag{A3}$$

C Implementation of Numerical Truncation

The most straightforward way to truncate Eq. 7 at $k = M$ is to neglect the exchange terms between c_M and c_{M+1}, assuming a negligible contribution for $k > M$ and essentially imposing a "no-flux" boundary condition. This leads to the following equation for the boundary term $c_M(t)$:

$$\frac{dc_M(t)}{dt} = \frac{\gamma(t)}{\Omega} c_{M-1} + p(M-1)c_{M-1} - \mu(N)Mc_M. \tag{A4}$$

This formulation, however, introduces a truncation error in Eq. 1 if we define $N = \sum_{k=1}^{M} kc_k$. The neglected terms leave a small loss of total cell count in dN/dt. An alternative implementation of the truncation is adding these small loss terms to the boundary equation:

$$\frac{dc_M(t)}{dt} = \frac{\gamma(t)}{\Omega} \left(c_{M-1} + \frac{c_M}{M} \right) + p(M-1)c_{M-1} + pc_M - \mu(N)Mc_M, \tag{A5}$$

thus preserving the total cell count N. However, for Eq. A5 the truncation error shows up in the total number of clonal types $\Omega = \sum_{k=0}^{M} c_k$, as the terms added to Eq. A5 to preserve N artificially introduce new clonal types into the model. In contrast, Ω is preserved with the implementation of Eq. A4. If $M \to \infty$, the truncation errors for both implementations go to zero at $\sim 1/M$, and the two implementations become equivalent. Assuming sufficiently large M, the truncation errors can be negligible in the context of $\gamma(t) > 0$ or have minimal cumulative effects within a limited duration, such as a human lifetime, on which our investigations in this paper have primarily focused.

In this paper, we adopt, for simplicity, Eq. A4 to numerically truncate Eq. 7. Note that this choice may seem "natural" if one regards M as the carrying capacity, making it reasonable for c_M to have zero proliferation rate. However, the full mechanisms associated with the carrying capacity are far more sophisticated than simply eliminating the proliferation of c_M. Not only should the proliferation rate of c_M go to zero, the proliferation rate of the other c_k should also have a k dependence. The k dependence may be weak for small k, but as $k \to M$, the proliferation rate should attenuate significantly. The probability that $c_{k \to M}$ will proliferate should be very small, as it is highly likely that there exist other smaller clones to push the total cell count up to the carrying capacity, prohibiting further proliferation. The k-dependent proliferation rate will yield a natural truncation threshold at the carrying capacity. However, such a sophisticated k dependence of the proliferation rate is beyond the scope of this paper. Our assumption here is simply that the truncation errors introduced by Eq. A4 are numerically negligible and not biologically significant.

D Steady States of the Autonomous Equations

If we fix $\gamma(t) = \gamma_0$, Eqs. 1, 7, and A4 become autonomous and admit the following steady-state solution:

$$c_1^{ss} = \gamma_0 \left[\frac{\gamma_0}{\Omega} \sum_{i=1}^{M} \frac{1}{i! \mu(N_{ss})^{i-1}} \left(\prod_{j=1}^{i-1} \left[\frac{\gamma_0}{\Omega} + jp \right] \right) + \mu(N_{ss}) \right]^{-1}, \qquad (A6)$$

$$c_k^{ss} = \frac{c_1^{ss}}{k! \mu(N_{ss})^{k-1}} \left(\prod_{n=1}^{k-1} \left[\frac{\gamma_0}{\Omega} + np \right] \right), \qquad (A7)$$

where N_{ss} is the total population at steady state, given by the unique positive root of the cubic:

$$c(N; \gamma_0) = (p_0 - (\mu_0 + \mu_1)) N^3 + \gamma_0 N^2 + (p_0 - \mu_0) K^2 N + \gamma_0 K^2. \qquad (A8)$$

When $\gamma_0 = 0, c(N; 0)$ has three real roots, $N = 0, \pm \sqrt{((p - \mu_0) K^2)/(\mu_0 + \mu_1 - p)}$. The positive steady-state solution, which we denote by $N_{ss}(0)$, is stable and the zero solution unstable, under the parameter restrictions described in Sect. 2.1. We now demonstrate that even though Eqs. A6, A7 indicate that each $c_k^{ss} \to 0$ as $\gamma_0 \to 0$,

the quantity $\lim_{M \to \infty} \sum_{k=1}^{M} k c_k^{ss}$ converges to a positive value qualitatively consistent with $N_{ss}(0)$ as $\gamma_0 \to 0$.

Proposition D *The steady-state solutions c_k^{ss}, as given in Eqs. A6, A7, satisfy*

$$\lim_{\gamma_0 \to 0} \lim_{M \to \infty} \sum_{k=1}^{M} k c_k^{ss} > 0.$$

Proof We seek to derive upper and lower bounds, $U(\gamma_0)$, $L(\gamma_0)$, which satisfy:

$$L(\gamma_0) \le \lim_{M \to \infty} \sum_{k=1}^{M} k c_k^{ss} \le U(\gamma_0),$$

for $\gamma_0 > 0$, and $\lim_{\gamma_0 \to 0} U(\gamma_0) \ge \lim_{\gamma_0 \to 0} L(\gamma_0) > 0$. We first establish two small results, which will be used later on: □

Proposition D1 *For $\mu = \mu(N_{ss}(\gamma_0))$, $\lim_{\gamma_0 \to 0} \frac{d\mu}{d\gamma_0} > 0$.*

Proof Recalling that $\mu = \mu(N_{ss}(\gamma_0)) = \mu_0 + \mu_1(N_{ss}(\gamma_0)^2/(N_{ss}(\gamma_0)^2 + K^2))$, we have

$$
\begin{aligned}
\frac{d\mu}{d\gamma_0} &= \frac{d\mu}{dN_{ss}} \frac{dN_{ss}}{d\gamma_0} \\
&= \frac{2\mu_1 K^2 N_{ss}}{(N_{ss}^2 + K^2)^2} \left[\frac{-(N_{ss}^2 + K^2)}{3(p_0 - (\mu_0 + \mu_1))N_{ss}^2 + 2\gamma_0 N_{ss} + (p_0 - \mu_0)K^2} \right] \\
&= \frac{-2\mu_1 K^2 N_{ss}}{(N_{ss}^2 + K^2) \left[3(p_0 - (\mu_0 + \mu_1))N_{ss}^2 + 2\gamma_0 N_{ss} + (p_0 - \mu_0)K^2 \right]}
\end{aligned}
$$

where we computed the derivative $\frac{dN_{ss}}{d\gamma_0}$ implicitly from the expression $c(N_{ss}(\gamma_0); \gamma_0) = 0$. From the explicit form $N_{ss}(0) = \sqrt{(p_0 - \mu_0)K^2/((\mu_0 + \mu_1) - p_0)}$, we have

$$
\begin{aligned}
\lim_{\gamma_0 \to 0} \frac{d\mu}{d\gamma_0} &= \frac{-2\mu_1 K^2 N_{SS}(0)}{(N_{SS}(0)^2 + K^2) \left[3(p_0 - (\mu_0 + \mu_1))N_{SS}(0)^2 + (p_0 - \mu_0)K^2 \right]} \\
&= \frac{-2\mu_1 K^2 N_{SS}(0)}{(N_{SS}(0)^2 + K^2) \left[-2(p_0 - \mu_0)K^2 \right]} \\
&> 0.
\end{aligned}
$$

□

Proposition D2 *For $f(p/\mu(N_{ss}(\gamma_0)); \gamma_0) = \frac{\gamma_0}{p\Omega} \left(1 - \frac{p}{\mu(N_{ss}(\gamma_0))} \right)^{-\frac{\gamma_0}{p\Omega} - 1}$, $\lim_{\gamma_0 \to 0} f(p/\mu(N_{ss}(\gamma_0)); \gamma_0) > 0$.*

Proof We write the function $f(p/\mu(N_{ss}(\gamma_0)); \gamma_0)$ as a product of two functions as follows:

$$f(p/\mu(N_{ss}(\gamma_0)); \gamma_0) = \frac{\gamma_0}{p\Omega}\left(1 - \frac{p}{\mu(N_{ss}(\gamma_0))}\right)^{-\frac{\gamma_0}{p\Omega}-1}$$

$$= \left(1 - \frac{p}{\mu(N_{ss}(\gamma_0))}\right)^{-\frac{\gamma_0}{p\Omega}} \frac{\gamma_0}{p\Omega}\left(1 - \frac{p}{\mu(N_{ss}(\gamma_0))}\right)^{-1}$$

$$= A(\gamma_0)B(\gamma_0).$$

We define $A_0 = \lim_{\gamma_0 \to 0} A(\gamma_0)$ and $B_0 = \lim_{\gamma_0 \to 0} B(\gamma_0)$, and compute A_0 and B_0:

$$\ln(A_0) = \lim_{\gamma_0 \to 0} \frac{-\gamma_0}{p\Omega} \ln\left(1 - \frac{p}{\mu(N_{ss}(\gamma_0))}\right)$$

$$= -\frac{1}{p\Omega} \lim_{\gamma_0 \to 0} \gamma_0 \ln\left(1 - \frac{p}{\mu(N_{ss}(\gamma_0))}\right)$$

$$= \frac{1}{p\Omega} \lim_{\gamma_0 \to 0} \gamma_0^2 \left(1 - \frac{p}{\mu(N_{ss}(\gamma_0))}\right)^{-1} \frac{d}{d\gamma_0}\left(-\frac{p}{\mu(N_{ss}(\gamma_0))}\right)$$

$$= \frac{1}{p\Omega} \lim_{\gamma_0 \to 0} \gamma_0^2 \left[1 - \frac{p}{\mu(N_{ss}(\gamma_0))}\right]^{-1} \left[p\mu(N_{ss}(\gamma_0))^{-2} \frac{d\mu}{d\gamma_0}\right]$$

$$= \frac{1}{p\Omega} \lim_{\gamma_0 \to 0} \left[\frac{\gamma_0^2 p \frac{d\mu}{d\gamma_0}}{\mu(N_{ss}(\gamma_0))^2 - p\mu(N_{ss}(\gamma_0))}\right]$$

$$= \frac{1}{\Omega} \lim_{\gamma_0 \to 0} \left[\frac{2\gamma_0 \frac{d\mu}{d\gamma_0} + \gamma_0^2 \frac{d^2\mu}{d\gamma_0^2}}{(2\mu - p)\frac{d\mu}{d\gamma_0}}\right]$$

$$= \frac{1}{\Omega} \left[\frac{2\gamma_0 \lim_{\gamma_0 \to 0} \frac{d\mu}{d\gamma_0} + \gamma_0^2 \lim_{\gamma_0 \to 0} \frac{d^2\mu}{d\gamma_0^2}}{p \lim_{\gamma_0 \to 0} \frac{d\mu}{d\gamma_0}}\right],$$

where we used that $\mu(N_{ss}(\gamma_0)) \to p$ as $\gamma_0 \to 0$. From Proposition D1, $\lim_{\gamma_0 \to 0} \frac{d\mu}{d\gamma_0} > 0$, and a similar computation shows that $\lim_{\gamma_0 \to 0} \frac{d^2\mu}{d\gamma_0^2} \in \mathbf{R}$. Thus, $\ln(A_0) \in \mathbf{R}$, and $A_0 > 0$. Now,

$$B_0 = \lim_{\gamma_0 \to 0} \frac{\gamma_0}{p\Omega}\left(1 - \frac{p}{\mu(N_{ss}(\gamma_0))}\right)^{-1}$$

$$= \lim_{\gamma_0 \to 0} \frac{(\gamma_0/p\Omega)}{\left(1 - \frac{p}{\mu(N_{ss}(\gamma_0))}\right)}$$

$$= \lim_{\gamma_0 \to 0} \frac{(1/p\Omega)}{p\mu(N_{ss}(\gamma_0))^{-2} \frac{d\mu}{d\gamma_0}}$$

$$= \lim_{\gamma_0 \to 0} \frac{\mu(N_{ss}(\gamma_0))^2}{p^2 \Omega \frac{d\mu}{d\gamma_0}}$$

$$> 0.$$

Thus, $\lim_{\gamma_0 \to 0} \frac{\gamma_0}{p\Omega} \left(1 - \frac{p}{\mu(N_{ss})}\right)^{-\frac{\gamma_0}{p\Omega}-1} = A_0 B_0 > 0.$

We now resume the proof of Proposition D. We first derive upper and lower bounds on the term c_1^{ss}, to simplify calculations. From the nonnegativity of the parameters and coefficient functions, and the form in Eq. A6, $c_1^{ss} \le \gamma_0/\mu_0$, independent of M. To derive an M-independent lower bound on c_1^{ss}, we observe that the sum in the denominator of Eq. A6 satisfies

$$\frac{\gamma_0}{\Omega} \sum_{i=1}^{M} \frac{1}{i!\mu(N_{ss}(\gamma_0))^{i-1}} \left(\prod_{j=1}^{i-1} \left[\frac{\gamma_0}{\Omega} + jp\right]\right)$$

$$\le \sum_{i=1}^{M} \frac{1}{(i-1)!\mu(N_{ss}(\gamma_0))^{i-1}} \left(\prod_{j=0}^{i-1} \left[\frac{\gamma_0}{\Omega} + jp\right]\right)$$

$$= p \sum_{i=1}^{M} \frac{1}{(i-1)!} \left(\prod_{j=0}^{i-1} \left[\frac{\gamma_0}{p\Omega} + j\right]\right) \left(\frac{p}{\mu(N_{ss}(\gamma_0))}\right)^{i-1}$$

and that the sum on the right above is the Mth Taylor polynomial, S_{M,γ_0}, for the function $f(x; \gamma_0) = \frac{\gamma_0}{p\Omega}(1-x)^{\frac{-\gamma_0}{p\Omega}-1}$ expanded around $x = 0$ and evaluated at $x = \frac{p}{\mu(N_{ss}(\gamma_0))}$. The function $f(x; \gamma_0)$ is analytic in x away from $x = 1$, and in particular, the S_{M,γ_0} increases monotonically to $f(p/\mu(N_{ss}(\gamma_0)); \gamma_0)$. It follows that

$$\frac{1}{p} \sum_{i=1}^{M} \frac{1}{i!\mu(N_{ss}(\gamma_0))^{i-1}} \left(\prod_{j=0}^{i-1} \left[\frac{\gamma_0}{\Omega} + jp\right]\right) \le S_{M,\gamma_0} \le f\left(\frac{p}{\mu(N_{ss}(\gamma_0))}; \gamma_0\right) := f_{\gamma_0}$$

and thus that $c_1^{ss} \ge \gamma_0/(pf_{\gamma_0} + \mu_0 + \mu_1)$. After using the c_1^{ss} bounds in the expression for c_k^{ss}, we have

$$\frac{p\Omega}{pf_{\gamma_0} + \mu_0 + \mu_1} S_{M,\gamma_0} \le \sum_{k=1}^{M} kc_k^{ss} \le \frac{p\Omega}{\mu_0} S_{M,\gamma_0}$$

$$\longrightarrow \lim_{M \to \infty} \frac{p\Omega}{pf_{\gamma_0} + \mu_0 + \mu_1} S_{M,\gamma_0} \le \lim_{M \to \infty} \sum_{k=1}^{M} kc_k^{ss} \le \lim_{M \to \infty} \frac{p\Omega}{\mu_0} S_{M,\gamma_0}$$

$$\longrightarrow \frac{p\Omega}{pf_{\gamma_0} + \mu_0 + \mu_1} f_{\gamma_0} \le \lim_{M \to \infty} \sum_{k=1}^{M} kc_k^{ss} \le \frac{p\Omega}{\mu_0} f_{\gamma_0}.$$

Now we let $L(\gamma_0) = \frac{p\Omega}{pf_{\gamma_0}+\mu_0+\mu_1} f_{\gamma_0}$ and $U(\gamma_0) = \frac{p\Omega}{\mu_0} f_{\gamma_0}$. From Proposition D2, $\lim_{\gamma_0 \to 0} f_{\gamma_0} > 0$, so $\lim_{\gamma_0 \to 0} L(\gamma_0)$, $\lim_{\gamma_0 \to 0} U(\gamma_0) > 0$, and Proposition D follows.

$\square$

E Convergence and Stability of c_k When $\gamma(t) \to 0$

In this section, we will prove that solutions c_k to our ODE system initialized sufficiently close to $\vec{0}$ converge to $\vec{0}$ as $t \to \infty$. Denote by (P) the "perturbed" ODE system given by Eqs. 7, A4, with $\gamma(t) = \gamma_0 e^{-at}$, and by (U) the "unperturbed" ODE system resulting from the alternate choice $\gamma(t) \equiv 0$. For the sake of generality, we omit previous assumptions about the form of the functions $p(N)$, $\mu(N)$, except that $p(0)$, $\mu(0) > 0$. Additionally, in this section, we regard the term N that appears in the ODEs as $\sum_{k\geq1} kc_k$ instead of its own variable and thus do not explicitly include Eq. 1 in our analysis as shown in "Appendix D." Note that the residual $N - \sum_{k\geq1} kc_k \to 0$ as $M \to \infty$. We begin by noting that the unperturbed system (U) has steady state $c_k^U(t) \equiv 0$ for $k \geq 1$. To analyze the stability of this steady state, we consider the linearization of (U) around this steady state, which is represented by the $M \times M$ matrix we call $\mathbf{L_U}$ ($\mathbf{L_U} = (l_{ij})_{1\leq i,j\leq M}$). The components l_{ij} of $\mathbf{L_U}$ are given explicitly by:

$$l_{ij} = \begin{cases} -j(p(0)+\mu(0)), & \text{if } i = j \leq M-1 \\ -M\mu(0), & \text{if } i = j = M \\ j\mu(0), & \text{if } i = j-1; \ 2 \leq j \leq M \\ jp(0), & \text{if } i = j+1; \ 1 \leq j \leq M-1 \\ 0, & \text{otherwise} \end{cases} \tag{A9}$$

Although the matrix is tridiagonal, it is high-dimensional, and thus, its eigenvalues cannot be computed analytically. However, we may nevertheless demonstrate that all eigenvalues possess strictly negative real part, indicating that the zero solution is asymptotically stable. To do this, we use Gershgorin's circle theorem to show that if there exists an eigenvalue $\lambda \in \mathbf{C}$ satisfying $\Re(\lambda) \geq 0$, then $\lambda = 0$. We then verify that $\lambda = 0$ is never an eigenvalue of $\mathbf{L_U}$, by directly demonstrating that $\mathbf{L_U}$ has linearly independent rows.

Proposition E *All eigenvalues $\lambda \in \mathbf{C}$ of the matrix $\mathbf{L_U}$ satisfy $\Re\lambda < 0$, so that the zero solution of (U) is asymptotically stable.*

We first apply Gershgorin's circle theorem to the columns of the matrix $\mathbf{L_U}$ to conclude that all eigenvalues $\lambda \in \mathbf{C}$ of the truncated system (finite M) are contained within the following union of disks:

$$\left(\bigcup_{i=1}^{M-1} \{\lambda \in \mathbf{C} : |\lambda + i(p(0) + \mu(0))| \leq i(p(0) + \mu(0))\} \right) \bigcup \{\lambda \in \mathbf{C} : |\lambda + M\mu(0)| \leq M\mu(0)\}, \tag{A10}$$

where we have used the fact that $\{\lambda \in \mathbf{C} : |\lambda + D| \leq D\} \subset \{\lambda \in \mathbf{C} : |\lambda + (D + \epsilon)| \leq D + \epsilon\}$ for $D, \epsilon > 0$. Given the assumption that $p(0), \mu(0) > 0$, each of these disks is tangent to the line $\Re\lambda = 0$ at $\lambda = 0$ and otherwise lies entirely in the half plane $\Re\lambda < 0$. Thus, $\mathbf{L_U}$ can only possess an eigenvalue λ satisfying $\Re\lambda = 0$ if $\lambda = 0$ is itself an eigenvalue. We next verify that $\lambda = 0$ is never an eigenvalue of $\mathbf{L_U}$ directly, by establishing the linear independence of the rows of $\mathbf{L_U}$.

Let us assume that there exist scalars $a_1, a_2, \ldots, a_M$, such that $\sum_{j=1}^{M} a_j \left(l_{ij} - 0\right) = 0$ for all $1 \leq i \leq M$. Hence, a normalized vector $\mathbf{a} = (a_1, a_2, \ldots, a_M)$ represents the eigenvector of the zero eigenvalue. For $i = 1$, we find that $2a_2\mu(0) - a_1(p(0) + \mu(0)) = 0$, so that $a_2 = 2^{-1}\mu(0)^{-1}(p(0) + \mu(0))a_1$. By moving on to larger i, we can recursively derive $a_i = \Theta_i a_1$ for all $2 \leq i \leq M$ with a proportional constant coefficient Θ_i. Moreover, $\sum_{i=1}^{M} \sum_{j=1}^{M} a_j l_{ij} = -a_1\mu(0) = 0$, leading to $a_1 = 0$ given that $\mu(0) > 0$. If $a_1 = 0$, $\mathbf{a} \equiv 0$, and a nonzero eigenvector does not exist, implying that zero is not among the eigenvalues of the $M \times M$ matrix $\mathbf{L_U}$. We thus conclude that all eigenvalues λ of the matrix $\mathbf{L_U}$ satisfy $\Re(\lambda) < 0$, and the zero solution of (U) is asymptotically stable for Eq. 7 truncated using Eq. A4 at an arbitrarily large M. Note that the proof in Eq. A10 does not hold if we use the alternative truncation formula Eq. A5. By forcing all cells to remain below the truncation threshold M, it is not possible for all c_k to go to zero with a finite M. For the alternative truncation, the stable steady-state solution is $c_k = 2N_{ss}/(M(M + 1))$, which nevertheless goes to zero as $M \to \infty$.

We next proceed to demonstrate that the uniform asymptotic stability of the zero solution ($c_k^U(t) \equiv 0$ for $k \geq 1$) of the unperturbed system (U) confers a similar notion of "stability" on the perturbed system (P). In particular, the uniform asymptotic stability of the system (U), in conjunction with the exponential decay of the function $\gamma(t)$, implies that solutions of the perturbed system (P) also converge to zero in magnitude, in a sense to be made more precise later on. Here let us simplify our notation by writing (U) as $d\mathbf{c}/dt = \mathbf{f}(\mathbf{c})$, where $\mathbf{c} \equiv (c_1, c_2, \ldots, c_M)$. The autonomous term $\mathbf{f}(\mathbf{c})$ consists of cell proliferation and death. Correspondingly, we express (P) as $d\mathbf{c}/dt = \mathbf{f}(\mathbf{c}) + \mathbf{g}(t, \mathbf{c})$, where the nonautonomous term $\mathbf{g}(t, \mathbf{c})$ describes thymic export that depends explicitly on the argument t. We appeal to results of Strauss and Yorke in (1967), in particular their Theorem 4.6, which we may invoke to prove that the solution of the perturbed system $\mathbf{c}^P(t) \to 0$ if the unperturbed and perturbed systems (U) and (P) satisfy the following conditions:

1. The zero solution ($\mathbf{c}^U(t) \equiv 0$) of the unperturbed system (U) is uniformly asymptotically stable.
2. The autonomous term $\mathbf{f}(\mathbf{c})$ is C^1.
3. There exists $r > 0$ such that if $|\mathbf{c}| \leq r$, then $|\mathbf{g}(t, \mathbf{c})| \leq \eta(t)$ for all $t \geq 0$ where $G(t) := \int_t^{t+1} \eta(s)ds \to 0$ as $t \to \infty$. (Here, we use the norm $|\mathbf{c}| = \sum_{i=1}^{M} |c_i|$.)

We now verify Conditions 1–3. Condition 1 follows immediately from the previous discussion, and the fact that for an autonomous system, asymptotic stability and uniform asymptotic stability are equivalent. Condition 2 is trivial. To verify Condition 3, we must construct a suitable function $\eta(t)$, using the definition of the function $g(t, \mathbf{c})$:

$$\begin{aligned}
|\mathbf{g}(t, \mathbf{c})| &= \left| \frac{\gamma_0 e^{-at}}{\Omega} \left(\Omega - \sum_{j=1}^{M} c_j - c_1 \right) \right| + \sum_{j=2}^{M-2} \left| \frac{\gamma_0 e^{-at}}{\Omega} \left(c_j - c_{j+1} \right) \right| \\
&\quad + \left| \frac{\gamma_0 e^{-at}}{\Omega} c_{M-1} \right| \\
&\leq \frac{\gamma_0 e^{-at}}{\Omega} \left(|\Omega| + \left(\sum_{i=1}^{M} |c_i| \right) + |c_1| \right) + \sum_{j=2}^{M-2} \frac{\gamma_0 e^{-at}}{\Omega} \left(|c_j| + |c_{j+1}| \right) \\
&\quad + \frac{\gamma_0 e^{-at}}{\Omega} |c_{M-1}| \\
&\leq \frac{\gamma_0 e^{-at}}{\Omega} \left(\Omega + 3 \sum_{i=1}^{M-1} |c_i| \right) \\
&\leq \frac{\gamma_0 e^{-at}}{\Omega} \left(\Omega + 3|\mathbf{c}| \right) \\
&= \gamma_0 e^{-at} \left(1 + \frac{3}{\Omega} |\mathbf{c}| \right)
\end{aligned} \tag{A11}$$

Thus, $|\mathbf{g}(t, \mathbf{c})| \leq \gamma_0 e^{-at} \left(1 + \frac{3}{\Omega} |\mathbf{c}| \right)$, and for a given choice of $r > 0$, we may define $\eta_r(t) := \gamma_0 e^{-at} \left(1 + \frac{3r}{\Omega} \right)$. From the exponential form of $\eta_r(t)$, it is clear that $\lim_{t \to \infty} \int_t^{t+1} \eta_r(s) ds = 0$. Moreover, not only does there exist a single choice of $r > 0$ that produces a suitable $\eta_r(t)$, but *any* choice of r produces a suitable $\eta_r(t)$.

From Theorem 4.6 in Strauss and Yorke (1967), we may conclude that for any $T_0 \geq 0$, there exists a $\delta_0 > 0$ such that if $t_0 \geq T_0$ and $|\mathbf{c}^P(t_0)| \leq \delta_0$, then the solution of the perturbed problem, $\mathbf{c}^P(t)$, passing through $(t_0, \mathbf{c}^P(t_0))$ converges to zero in magnitude as $t \to \infty$. Here the proof of convergence holds for any sufficiently smooth function $\gamma(t) \to 0$. Given Eq. 7 truncated at an arbitrarily large threshold M, all c_k decline with the decaying thymic export as $t \to \infty$. While the total cell count is preserved by proliferation driving all cells above the truncation threshold and out of the truncated system through truncation errors, the mean-field approximation breaks down at the limit $\gamma(t)/\mu \to 1/\Omega \ll 1$, and Eq. 7 no longer accurately describes the real biology. Nonetheless, our analysis here describes the decline of the number of T cell clones with decaying $\gamma(t)$ as $t \to \infty$, before the mean-field approximation breaks down.

F Computation of Expected Sample Clonal Size Distribution

In this section, we detail the derivation of Eq. 11, the explicit expression for $\mathbb{E}[c_k^Y]$. We begin with Eq. 10,

$$\mathbb{E}[c_k] = \sum_{j=1}^{R} j P \left(c_k^Y = j \right). \tag{A12}$$

Each term $P\left(c_k^Y = j\right)$ in Eq. A12 can itself be expanded as a sum over all the ways to choose the j clones that are of size k. For a sample containing exactly Z clones of size k, we introduce the following Z-tuple notation, for $Z \in \mathbb{N}$:

$$I_Z := \{\mathbf{i_Z} = (i_1, i_2, \ldots, i_Z) : i_j \in \{1, 2, \ldots, R\}, i_j < i_{j+1} \text{ for all } j\}.$$

where $\mathbf{i_Z}$ lists the indices of all the sample clones consisting of precisely k cells. Additionally, let y_i denote the size of the ith ordered sample clone, so that $y_{i_1} = y_{i_2} = \cdots = y_{i_Z} = k$, but no other sample clone consists of k cells. Note that in $\mathbf{i_Z}$, clones are listed in numerical order, due to the assumption $i_j < i_{j+1}$, in order to avoid repetition (e.g., in I_2, (i_1, i_2) should be indistinct from (i_2, i_1), and this pair should not be counted twice, as the significance is in which clone numbers are listed at all, and not the order in which they are written.) With this, let $P(\mathbf{i_Z}, k)$ denote the probability that there are precisely Z clones of size k in the sample, and that their clone numbers are listed in the vector $\mathbf{i_Z}$. Additionally, for $s \in \mathbb{N}$, denote by $I_{Z,s} \subset I_Z$ the collection of all $\mathbf{i_Z} \in I_Z$ such that $i_{z^*} = s$ for some $z^* \in \{1, 2, \ldots, Z\}$. Essentially, we are imposing the assumption that the sth clone specifically belongs somewhere in the list $\mathbf{i_{Z,s}}$. Explicitly, we may write $I_{Z,s}$ as:

$$I_{Z,s} = \{\mathbf{i_{Z,s}} = (i_1, \ldots, i_{z^*-1}, i_{z^*} = s, i_{z^*+1}, \ldots, i_Z) : i_j \in \{1, 2, \ldots, R\},$$
$$i_j < i_{j+1} \text{ for all } j\}. \tag{A13}$$

We define $P(\mathbf{i_{Z,s}}, k)$ as the probability that there are precisely Z clones of size k, with clone numbers listed in $\mathbf{i_{Z,s}}$, recalling that the sth clone is in the list. We may further simplify Eq. A12 with this notation, rearranging sums by strategically regrouping clone size distributions that share a common size k clone.

$$\mathbb{E}[c_k] = \sum_{j=1}^{R} j P(c_k^Y = j)$$

$$= \sum_{j=1}^{R} j \left(\sum_{\mathbf{i_j} \in I_j} P(\mathbf{i_j}, k) \right)$$

$$= \sum_{s=1}^{R} \left(\sum_{j=1}^{R} \sum_{\mathbf{i_{j,s}} \in I_{j,s}} P(\mathbf{i_{j,s}}, k) \right)$$

$$= \sum_{s=1}^{R} P(y_s = k). \tag{A14}$$

The terms of the final sum in Eq. A14 give the probability that the sth clone is of size k, independent of any other information about the sampling. This probability is easy to compute and given by:

$$P(y_s = k) = \frac{1}{\binom{N}{Y}} \binom{n_s}{k} \binom{N - n_s}{Y - k}. \tag{A15}$$

Inserting Eq. A15 into Eq. A14, we obtain a simple expression for the expected sample clone size distribution:

$$\mathbb{E}[c_k] = \sum_{s=1}^{R} \frac{1}{\binom{N}{Y}} \binom{n_s}{k} \binom{N - n_s}{Y - k}. \tag{A16}$$

We can further simplify Eq. A16 by recognizing that the term $\binom{n_s}{k}$ is nonzero only if $n_s \geq k$. We can thus rewrite Eq. A16 in terms of the true clone size distribution $\{c_l^N\}_{l=1}^{R}$ as:

$$\mathbb{E}[c_k] = \sum_{l=k}^{R} \frac{1}{\binom{N}{Y}} c_l^N \binom{l}{k} \binom{N - l}{Y - k}. \tag{A17}$$

References

Appay V, Sauce D (2014) Naive T cells: The crux of cellular immune aging? Expe Gerontol 54:90–93

Bains I, Antia R, Callard R, Yates AJ (2009a) Quantifying the development of the peripheral naive CD4+ T-cell pool in humans. Immunobiology 113(22):5480–5487

Bains I, Thiébaut R, Yates AJ, Callard R (2009b) Quantifying thymic export: Combining models of naive T cell proliferation and TCR excision circle dynamics gives an explicit measure of thymic output. J Immunol 183(7):4329–4336

Berzins SP, Boyd R, Miller JF (1998) The role of the thymus and recent thymic migrants in the maintenance of the adult peripheral lymphocyte pool. J Exp Med 187(11):1839–1848

Bradley LM, Haynes L, Swain SL (2005) IL-7: maintaining T-cell memory and achieving homeostasis. Trends Immunol 26(3):172–176

Brass D, McKay P, Scott F (2014) Investigating an incidental finding of lymphopenia. Br Med J 348:1–3

Britanova OV, Putintseva EV, Shugay M, Merzlyak EM, Turchaninova MA, Staroverov DB, Bolotin DA, Lukyanov S, Bogdanova EA, Mamedov IZ, Lebedev YB, Chudakov DM (2014) Age-related decrease in TCR repertoire diversity measured with deep and normalized sequence profiling. J Immunol 192(6):2689–2698

Chao A (1984) Nonparametric estimation of the number of classes in a population. Scand J Stat 11(4):265–270

Chao A, Lee SM (1992) Estimating the number of classes via sample coverage. J Am Stat Assoc 87(417):210–217

Colwell RK, Coddington JA (1994) Estimating terrestrial biodiversity through extrapolation. Philos Trans R Soc B 345(1311):101–118

de Boer RJ, Perelson AS (2013) Quantifying T lymphocyte turnover. J Theor Biol 327:45–87

den Braber I, Mugwagwa T, Vrisekoop N, Westera L, Mögling R, de Boer AB, Willems N, Schrijver EHR, Spierenburg G, Gaiser K, Mul E, Otto SA, Ruiter AF, Ackermans MT, Miedema F, Borghans JAM, de Boer RJ, Tesselaar K (2012) Maintenance of peripheral naive T cells is sustained by thymus output in mice but not humans. Immunity 36:288–297

Desponds J, Mora T, Walczak A (2015) Fluctuating fitness shapes the clone-size distribution of immune repertoires. Proc Natl Acad Sci 113(2):274–279

Desponds J, Mayer A, Mora T, Walczak AM (2017) Population dynamics of immune repertoires. arXiv e-prints arXiv:1703.00226

Ewens W (1972) The sampling theory of selectively neutral alleles. Theor Popul Biol 3(1):87–112

Fagnoni FF, Vescovini R, Passeri G, Bologna G, Pedrazzoni M, Lavagetto G, Casti A, Franceschi C, Passeri M, Sansoni P (2000) Shortage of circulating naive CD8+ T cells provides new insights on immunodeficiency in aging. Blood 95(9):2860–2868

Fleming DM, Elliot AJ (2008) The impact of influenza on health and health care utilisation of elderly people. Vaccine 32(1):S1–S9

Fry TJ, Mackall CL (2005) The many faces of IL-7: from lymphopoesis to peripheral T cell maintenance. J Immunol 174(11):6571–6576

Gergely P (1999) Drug-induced lymphopenia. Drug Saf 21(2):91–100

Ginaldi L, Loreto MF, Corsi MP, Modesti M, de Martinis M (2001) Immunosenescence and infectious diseases. Microbes Infect 3(10):851–857

Globerson A, Effros RB (2000) Aging of lymphocytes and lymphocytes in the aged. Immunol Today 21(10):515–521

Goronzy JJ, Lee WW, Weyland CM (2007) Aging and T-cell diversity. Exp Gerontol 42(5):400–406

Goronzy JJ, Fang F, Cavanagh MM, Qi Q, Weyand CM (2015a) Naïve T cell maintenance and function in human aging. J Immunol 194(9):4073–4080

Goronzy JJ, Qi Q, Olshen RA, Weyland CM (2015b) High-throughput sequencing insights into T-cell receptor diversity in aging. Genome Med 7:1–3

Goyal S, Kim S, Chen ISY, Chou T (2015) Mechanisms of blood homeostasis: lineage tracking and a neutral model of cell populations in rhesus macaques. BMC Biol 13(85):1–14

Grossman SA, Ellsworth S, Campian J, Wild AT, Herman JM, Laheru D, Brock M, Balmanoukian A, Ye X (2015) Survival in patients with severe lymphopenia following treatment with radiation and chemotherapy for newly diagnosed solid tumors. J Natl Compr Cancer Netw 13(10):1225–1231

Gruver A, Hudson L, Sempowski J (2007) Immunosenescence of aging. J Pathol 211(2):144–156

Hapuarachchi T, Lewis J, Callard RE (2013) A mechanistic mathematical model for naive CD4 T cell homeostasis in healthy adults and children. Front Immunol 4(366):1–6

Hodes RJ, Hathcock KS, Np Weng (2002) Telomeres in T and B cells. Nat Rev Immunol 2:699–706

Jenkins MK, Chu HH, McLachlan JB, Moon JJ (2009) On the composition of the preimmune repertoire of T cells specific for peptide-major histocompatibility ligands. Annu Rev Immunol 28:275–294

Johnson PLF, Yates AJ, Goronzy JJ, Antia R (2012) Peripheral selection rather than thymic involution explains sudden contraction in naive CD4 T-cell diversity with age. PNAS 109(52):21432–21437

Johnson PLF, Goronzy JJ, Atia R (2014) A population biological approach to understanding the maintenance and loss of the T-cell repertoire during aging. Immunology 142(2):167–175

Laydon DJ, Bangham CRM, Asquith B (2015) Estimating T-cell repertoire diversity: limitations of classical estimators and a new approach. Philos Trans R Soc B 370(1675):1–11

Lythe G, Callard RE, Hoare RL, Molina-Par'ıs C (2016) How many TCR clonotypes does a body maintain? J Theor Biol 389:214–224

Marcou Q, Mora T, Walczak AM (2018) High-throughput immune repertoire analysis with IGoR. Nat Commun 9(1):561

Mason D (1998) A very high level of crossreactivity is an essential feature of the T-cell receptor. Trends Immunol 19(9):395–404

McElhaney JA, Dutz JP (2008) Better influenza vaccines for older people: What will it take? J Infect Dis 198(5):632–634

Mehr R, Perelson AS, Fridkis-Hareli M, Globerson A (1996) Feedback regulation of T cell development: manifestations in aging. Mech Ageing Dev 91(3):195–210

Mehr R, Perelson AS, Fridkis-Harelic M, Globersond A (1997) Regulatory feedback pathways in the thymus. Immunol Today 18(12):581–585

Metcalf D (1963) The autonomous behavior of normal thymus grafts. Aust J Exp Biol Med Sci 41:437–444

Mora T, Walczak A (2016) Quantifying lymphocyte receptor diversity. arXiv e-prints arXiv:1604.00487

Moro-García MA, Arias RA, López-Arrea C (2013) When aging reaches CD4+ T-cells: phenotypic and functional changes. Front Immunol 4(107):1–12

Morris EK, Caruso T, Buscot F, Fischer M, Hancock C, Maier TS, Meiners T, Müller C, Obermaier E, Prati D, Socher SA, Sonnemann I, Wäschke N, Wubet T, Wurst S, Rillig MC (2014) Choosing and using diversity indices: insights for biological applications from the German biodiversity exploratories. Ecol Evol 4:3514–3524

Murphy K (2012) Immunobiology. Garland Science, Taylor and Francis Group LLC, Routledge

Murray JM, Kaufmann GR, Hodgkin PD, Lewin SR, Kelleher AD, Davenport MP, Zaunders JJ (2003) Naive T-cells are maintained by thymic output in early ages but by proliferation without phenotypic change after age 20. Immunol Cell Biol 81(6):487–495

Naylor K, Li G, Vallejo AN, Lee WW, Koetz K, Bryl E, Witkowski J, Fulbright J, Weyand CM, Goronzy JJ (2005) The influence of age on T cell generation and TCR diversity. J Immunol 174(11):7446–7452

Np Weng, Levine BL, June CH, Hodes RJ (1995) Human naive and memory T lymphocytes differ in telomeric length and replicative potential. PNAS 92(24):11091–11094

Oakes T, Heather JM, Best K, Byng-Maddick R, Husovsky C, Ismail M, Joshi K, Maxwell G, Noursadeghi M, Riddell N, Ruehl T, Turner CT, Uddin I, Chain B (2017) Quantitative characterization of the T cell receptor repertoire of Naïve and memory subsets using an integrated experimental and computational pipeline which is robust, economical, and versatile. Front Immunol. https://doi.org/10.3389/fimmu.2017.01267

Poland GA, Langley J, Michel J, Van Damme P, Wicker S (2010) A global prescription for adult immunization: time is catching up with us. Vaccine 28(44):7137–7139

Pulko V, Davies JS, Martinez C, Lanteri MC, Busch MP, Diamond MS, Knox K, Busch ES, Sims PA, Sinari S, Billheimer D, Haddad EK, Murray KO, Wertheimer AM, Nikolich-Žugich J (2016) Human memory T cells with a naive phenotype accumulate with aging and respond to persistent viruses. Nat Immunol 17(8):966–975

Qi Q, Liu Y, Cheng Y, Glanville J, Zhang D, Lee JY, Olshen RA, Weyand CM, Boyd SD, Goronzy JJ (2014) Diversity and clonal selection in the human T-cell repertoire. Proc Natl Acad Sci 111(36):13139–13144

Reynolds J, Coles M, Lythe G, Molina-París C (2013) Mathematical model of naive T cell division and IL-7 survival thresholds. Front Immunol 4(434):1–13

Ribeiro RM, Perelson AS (2007) Determining thymic output quantitatively: using models to interpret experimental T-cell receptor excision circle (TREC) data. Immunol Rev 216(1):21–34

Rubinstein MP, Lind NA, Purton JF, Filippou P, Best JA, McGhee PA, Surh CD, Goldrath AW (2008) IL-7 and IL-15 differentially regulate CD8+ T-cell subsets during contraction of the immune response. Blood 112(9):3704–3712

Salam N, Rane S, Das R, Faulkner M, Gund R, Kandpal U, Lewis V, Prabhu HMS, Ranganathan V, Durdik J, George A, Rath S, Bal V (2013) T cell ageing: effects of age on development, survival, and function. Indian J Med Res 138(5):595–608

Saule P, Trauet J, Dutriez V, Lekeux V, Dessaint JP, Labalette M (2005) Accumulation of memory T cells from childhood to old age: central and effector memory cells in CD4+ versus effector memory and terminally differentiated memory cells in CD8+ compartment. Mech Ageing Dev 127(3):274–281

Shugay M, Bagaev DV, Turchaninova MA, Bolotin DA, Britanova OV, Putintseva EV, Pogorelyy MV, Nazarov VI, Zvyagin IV, Kirgizova VI, Kirgizov KI, Skorobogatova EV, Chudakov DM (2015) VDJtools: unifying post-analysis of T cell receptor repertoires. PLOS Comput Biol 11(11):1–16

Steinmann GG (1986) The human thymus, current topics in pathology, vol 75. Chap changes in the human thymus during aging. Springer, Berlin, Heidelberg, pp 43–88

Steinmann G, Klaus B, Müller-Hermelink H (1985) The involution of the ageing human thymic epithelium is independent of puberty. Scand J Immunol 22(5):563–575

Strauss A, Yorke JA (1967) Perturbation theorems for ordinary differential equations. J Differ Equ 3(1):15–30

Surh CD, Sprent J (2008) Homeostasis of naive and memory T cells. Immunity 29(6):848–862

Tan JT, Dudl E, LeRoy E, Murray R, Sprent J, Weinberg KI, Surh CD (2001) IL-7 is critical for homeostatic proliferation and survival of naive T cells. Proc Natl Acad Sci 98(15):8732–8737

Thomas-Crussels J, McElhaney JE, Aguado MT (2012) Report of the ad-hoc consultation on aging and immunization for a future who research agenda on life-course immunization. Vaccine 40(32):6007–6012

Trepel F (1974) Number and distribution of lymphocytes in man. Klinische Wochenschr 52(11):511–515

Vivien L, Benoist C, Mathis D (2001) T lymphocytes need IL-7 but not IL-4 or IL-6 to survive in vivo. Int Immunol 13(6):763–768

Vrisekoop N, den Braber I, de Boer AB, Ruiter AFC, Ackermans MT, van der Crabben SN, Schrijver EHR, Spierenburg G, Sauerwein HP, Hazenberg MD, de Boer RJ, Miedema F, Borghans JAM, Tesselaar K (2008) Sparse production but preferential incorporation of recently produced naive T-cells in the human peripheral pool. Proc Natl Acad Sci 105(16):6115–6120

Westera L, van Hoeven V, Drylewicz J, Spierenburg G, van Velzen JF, de Boer RJ, Tesselaar K, Borghans JAM (2015) Lymphocyte maintenance during healthy aging requires no substantial alterations in cellular turnover. Aging Cell 14(2):219–227

Westermann J, Pabst R (1990) Lymphocyte subsets in the blood: A diagnostic window on the lymphoid system? Immunol Today 11(11):406–410

Wick G, Dürr PJ, Berger P, Blasko I, Grubeck-Loebenstein B (2000) Diseases of aging. Vaccine 18(16):1567–1583

Xu S, Chou T (2018) Immigration-induced phase transition in a regulated multispecies birth-death process. J Phys A 51:425602

Yagger EJ, Ahmed M, Lanzer K, Randall TD, Woodland DL, Blackman MA (2008) Age-associated decline in T cell repertoire diversity leads to holes in the repertoire and impaired immunity to the influenza virus. J Exp Med 205(3):711–723

Yates AJ (2014) Theories and quantification of thymic selection. Front Immunol 5(13):1–15